nature nanotechnology

Article

https://doi.org/10.1038/s41565-024-01747-6

Combinatorial design of siloxane-incorporated lipid nanoparticles augments intracellular processing for tissue-specific mRNA therapeutic delivery

Received: 9 April 2023

Accepted: 8 July 2024

Published online: 1 October 2024

Check for updates

Lulu Xue[1,14], Gan Zhao[2,14], Ningqiang Gong[1,14], Xuexiang Han[1], Sarah J. Shepherd[1], Xinhong Xiong[3], Zebin Xiao[2], Rohan Palanki[1], Junchao Xu[1], Kelsey L. Swingle[1], Claude C. Warzecha[4], Rakan El-Mayta[1], Vivek Chowdhary[4], Il-Chul Yoon[1], Jingcheng Xu[1], Jiaxi Cui[3,5], Yi Shi[6], Mohamad-Gabriel Alameh[7,8], Karin Wang[9], Lili Wang[4], Darrin J. Pochan[6], Drew Weissman[7,8], Andrew E. Vaughan[2], James M. Wilson[4] & Michael J. Mitchell[1,8,10,11,12,13]

Systemic delivery of messenger RNA (mRNA) for tissue-specific targeting using lipid nanoparticles (LNPs) holds great therapeutic potential. Nevertheless, how the structural characteristics of ionizable lipids (lipidoids) impact their capability to target cells and organs remains unclear. Here we engineered a class of siloxane-based ionizable lipids with varying structures and formulated siloxane-incorporated LNPs (SiLNPs) to control in vivo mRNA delivery to the liver, lung and spleen in mice. The siloxane moieties enhance cellular internalization of mRNA-LNPs and improve their endosomal escape capacity, augmenting their mRNA delivery efficacy. Using organ-specific SiLNPs to deliver gene editing machinery, we achieve robust gene knockout in the liver of wild-type mice and in the lungs of both transgenic GFP and Lewis lung carcinoma (LLC) tumour-bearing mice. Moreover, we showed effective recovery from viral infection-induced lung damage by delivering angiogenic factors with lung-targeted Si_5-N14 LNPs. We envision that our SiLNPs will aid in the clinical translation of mRNA therapeutics for next-generation tissue-specific protein replacement therapies, regenerative medicine and gene editing.

Messenger RNA (mRNA)-based therapeutics have the potential to revolutionize vaccination[1,2], protein replacement therapies[3,4], cancer immunotherapies[5,6] and gene editing[7,8]. Recently, the US Food and Drug Administration approved two COVID-19 mRNA vaccines enabled by lipid nanoparticle (LNP) delivery systems comprised of an ionizable lipid, phospholipid, cholesterol and poly(ethylene glycol) (PEG)-lipid[9–11]. In clinical trials, LNPs encapsulating Cas9 mRNA and single guide RNA (sgRNA) targeting transthyretin (*TTR*) have demonstrated durable knockout of *TTR* to treat hereditary transthyretin amyloidosis[12,13]. In addition, emerging LNP formulations such as biodegradable LNPs[14,15], vitamin-derived LNPs[16], imidazole LNPs[17], dendrimer-like LNPs[18], heterocyclic LNPs[19], bisphosphonate LNPs[20] and biomimetic LNPs[21] have been evaluated in preclinical studies to increase the potency and minimize the toxicity of LNP-based therapeutics, highlighting the importance of developing ionizable lipids (lipidoids) for clinical applications. However, when administered

A full list of affiliations appears at the end of the paper. e-mail: mjmitch@seas.upenn.edu

systemically, LNPs preferentially accumulate in the liver, making extrahepatic delivery of mRNA challenging[22,23].

Recently, strategies including passive, active and endogenous targeting have been exploited to tune mRNA-LNP delivery to specific organs[22,24–26]. However, structure–activity relationships that link ionizable lipid structure with tissue-specific mRNA delivery in a single lipid library are not well established. To our knowledge, engineering a single synthetic LNP library with novel lipidoid chemical structures for liver-, lung- and spleen-targeted delivery upon systemic administration has not been demonstrated. Therefore, there is a substantial need for lipid-like materials whose chemical structures can be easily altered to mediate tissue-tropic delivery of mRNA therapeutics.

Owing to the high stability, low chemical reactivity and good biocompatibility of siloxane composites[27,28], herein, we used a combinatorial design approach to synthesize a library of 252 siloxane-incorporated lipidoids with varied siloxane amine core compositions and alkyl chain structures. These siloxane-incorporated lipidoids were used to formulate siloxane-incorporated LNPs (SiLNPs) to demonstrate structure-guided, systemic in vivo mRNA delivery. We show that the incorporation of a siloxane moiety into the lipidoid structure not only enhances the endocytosis of mRNA-LNPs but also improves their endosomal escape capacity, leading to greater mRNA delivery efficacy. Upon in vivo evaluation, we observed that minor structural alterations of siloxane-incorporated lipidoids can substantially alter organ tropism (Fig. 1a). Liver-, lung- and spleen-targeted SiLNPs show organ-specific transfection of various cell types including hepatocytes, Kupffer cells, endothelial cells (ECs), dendritic cells and splenic macrophages in an Ai14 mouse model. Using organ-specific SiLNPs to deliver CRISPR–Cas9-based gene editors, robust gene knockout in the liver of wild-type mice and in the lungs of transgenic GFP and Lewis lung carcinoma (LLC) tumour-bearing mice was achieved. In addition, lung-targeted SiLNPs delivering fibroblast growth factor-2 (FGF-2) mRNA increased vascular repair in a viral infection lung damage model. This study is a proof-of-concept demonstration that tuning in vivo LNP organ targeting can be achieved through incorporation of a siloxane moiety into the lipidoid structure, enabling the development of next-generation lipid-like materials for tissue-specific mRNA delivery.

Siloxane-incorporated lipidoids for in vitro mRNA delivery

As siloxane composites have been used in medical devices, cosmetics and drug delivery owing due to their low toxicity and high stability[27–29], we sought to explore whether these materials could be exploited to engineer highly stable and minimally toxic LNPs for mRNA delivery[10,11]. Combinatorial reactions between siloxane amines (Si_x) and epoxide-/ester-/amide bond-based alkylated tails (Cy/Oy/Ny) enabled the synthesis of 252 siloxane-based lipidoids[30] (Fig. 1b, Supplementary Schemes 1–5 and Supplementary Figs. 1–20). Each siloxane-incorporated lipidoid is denoted as Si_x-Cy/Si_x-Oy/Si_x-Ny, where '*x*' indicates the number of siloxane amine heads in this study and '*y*' represents the length of different alkyl chains.

To evaluate the structure–activity relationships of siloxane-incorporated lipidoids for mRNA delivery, SiLNPs encapsulating firefly luciferase (FLuc) mRNA were formulated and used to transfect human liver carcinoma cells (HepG2), a representative cell type for demonstrating the transfection efficacy of LNPs[31,32]. A library of 252 SiLNPs was formulated using a microfluidic device designed with herringbone features to induce chaotic mixing between the aqueous mRNA phase and the ethanol phase containing a unique siloxane-incorporated lipidoid, 1,2-dioleoyl-*sn*-glycero-3-phosphoethanolamine (DOPE), cholesterol and lipid-anchored PEG (C14PEG2K) at a molar ratio of 35:16:46.5:2.5 (Extended Data Fig. 1a–c), respectively. The resulting SiLNPs had a range of encapsulation efficiencies (EE) (60–93%) and hydrodynamic diameters (50–200 nm) with primarily monodisperse populations as indicated by a polydispersity index (PDI) less than 0.2 for approximately 70% of SiLNPs (Supplementary Tables 1–4).

Based on in vitro screening in HepG2 cells, we generated a heat map to elucidate which siloxane-incorporated lipidoid parameters influenced mRNA delivery efficacy by calculating a relative hit rate, which was defined as SiLNPs with relative luminescence units greater than 200 (Fig. 1c). We found that the number of silicon groups per lipidoid (Fig. 1d), the tail substitution number (Fig. 1e), tail length (Fig. 1f), tail type (Fig. 1g) and lipidoid core morphology impacted mRNA delivery efficacy (Fig. 1h). Moreover, greater mRNA transfection was achieved by introducing sulfur elements to functionalize the siloxane amine cores (Fig. 1i and Supplementary Fig. 21), perhaps owing to the antioxidant ability of the sulfur moiety[33]. Within this library, the Si_7-N12 LNP mediated up to 6-fold greater mRNA transfection than the gold-standard D-Lin-MC3-DMA (MC3) LNP (Supplementary Fig. 22a) and also demonstrated dose-dependent mRNA transfection (Supplementary Fig. 22b). To elucidate the impact of specific LNP components on in vitro mRNA delivery, as an illustrative example, we deliberately excluded DOPE from the LNP formulation. The exclusion of DOPE did not exert a substantial effect on particle size but significantly attenuated LNP transfection efficacy (Supplementary Fig. 23). These studies highlight the potential of siloxane-incorporated lipidoids for mRNA delivery in vitro, motivating us to further explore how the integration of a siloxane domain enhances mRNA delivery.

Siloxane incorporation improves intracellular processing

To demonstrate the precise role of the siloxane moiety on intracellular mRNA delivery, we used lipidoids with identical tail structures and head lengths, but lacking siloxane domains, as controls. Thus, the 213-N14 lipidoid was synthesized as a control for the Si_5-N14 lipidoid (Fig. 2a). To evaluate the efficacy of these two lipidoids for mRNA delivery, an endothelial cell line—immortalized human lung microvascular endothelial cells (iMVECs)—was used, given that blood vessels are a site for LNP interaction following systemic administration. First, intracellular uptake was investigated using the Si_5-N14 and 213-N14 LNPs formulated with Cy5-tagged mRNA (Fig. 2b). Si_5-N14 LNPs demonstrated significantly faster and greater cellular uptake than 213-N14 LNPs (Fig. 2c–f), which could be attributed to the relatively higher hydrophobicity (higher ALog *P* value) of Si_5-N14 (ref. 34) (Fig. 2a). However, this phenomenon was not observed in A549 and NIH/3T3 cell lines (Supplementary Fig. 24), indicating higher selectivity for endothelial cells.

Fig. 1 | A combinatorial library of siloxane-incorporated ionizable lipids with tunable structures for tissue-specific mRNA delivery. a, SiLNPs were formulated using a microfluidic mixing device each with a siloxane-incorporated lipidoid, helper lipid (DOPE), cholesterol and PEG-lipid (C14PEG2K). The resulting SiLNPs with different siloxane-incorporated lipidoid structures mediate in vivo tissue-specific mRNA delivery to the liver, lungs and spleen. **b**, Structures of the 12 siloxane amines and 21 alkyl tails used for combinatorial design and synthesis of the 252 siloxane-incorporated lipidoids. **c**, A heat map of luciferase expression following treatment of HepG2 cells with SiLNPs (5,000 cells, 10 ng luciferase mRNA, $n = 3$ biological independent samples). Hits were defined as siloxane-incorporated lipidoids with relative luminescence units greater than 200. **d**, Relative hit rate of SiLNPs by the number of silicon atoms per siloxane-incorporated lipidoid. **e**, Relative hit rate of SiLNPs by tail substitution number. **f**, Relative hit rate of SiLNPs by tail length. **g**, Relative hit rate of SiLNPs by tail type (epoxide-, ester- and amide bond-based tails). **h**, Relative hit rate of SiLNPs by siloxane amine core morphology among the core morphology-associated formulations. **i**, Relative hit rate of SiLNPs with and without the incorporation of sulfur atoms into the starting siloxane amines. Adding sulfur substantially enhanced in vitro mRNA delivery efficacy. 2Si-X represents siloxane-incorporated lipidoids with 2 Si atoms and 1 amine group (Si_1- versus Si_2-), and X-2Si-X represents siloxane-incorporated lipidoids with 2 Si atoms and 2 amine groups (Si_5- versus Si_6-).

https://doi.org/10.1038/s41565-024-01747-6

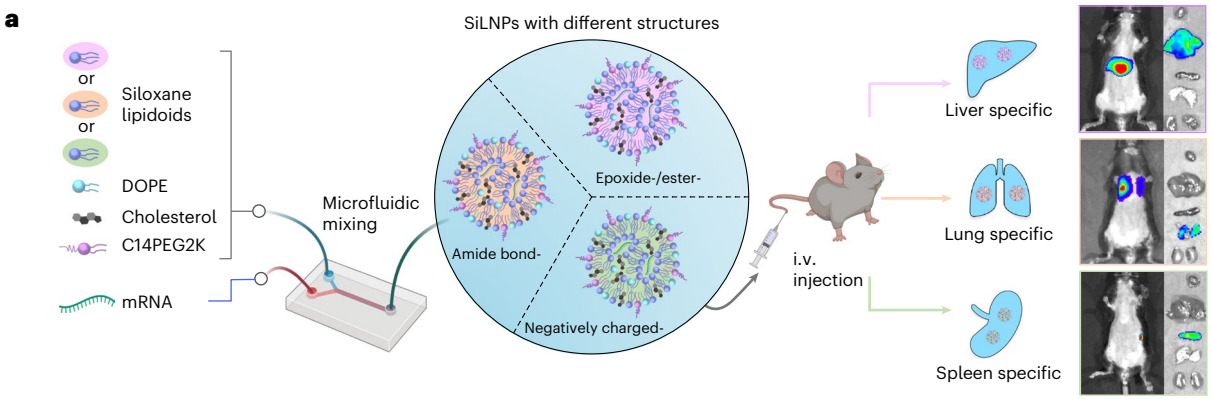

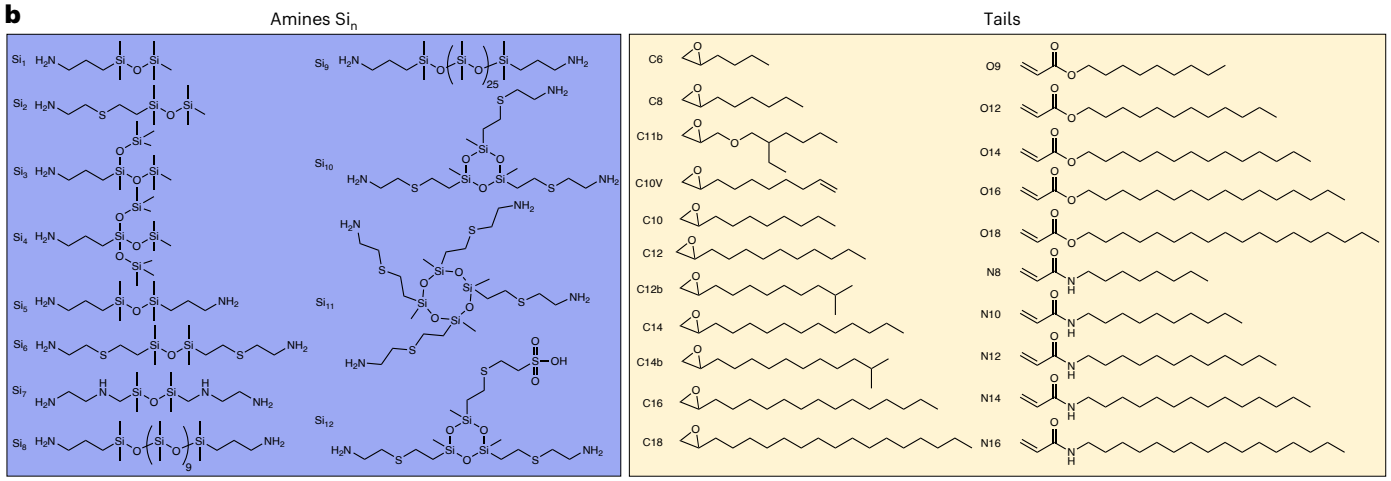

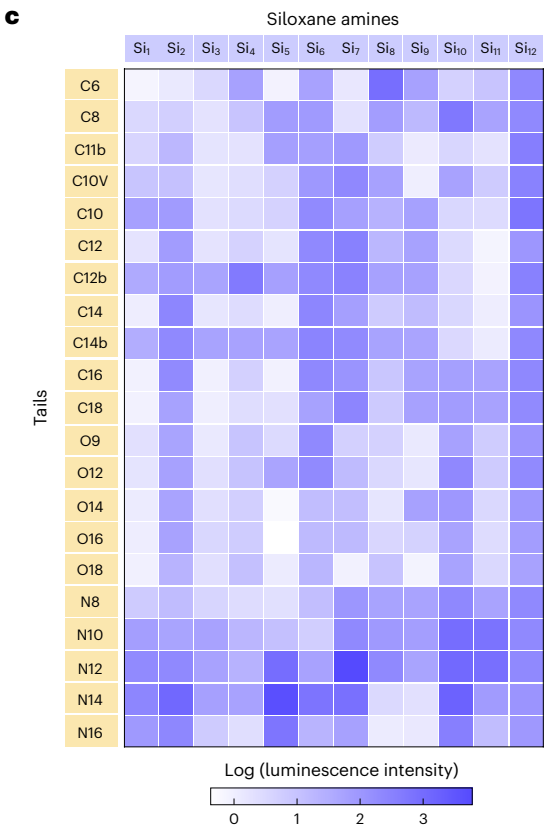

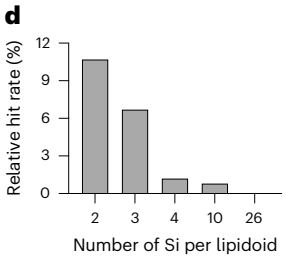

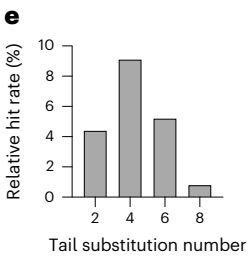

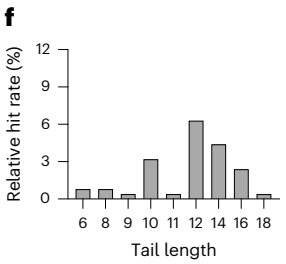

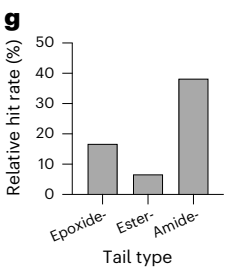

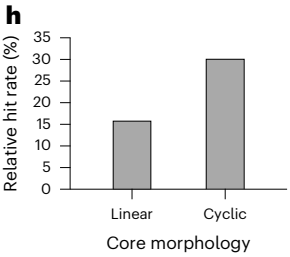

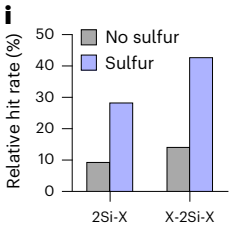

Furthermore, we investigated the effect of inhibiting various endocytosis pathways on LNP uptake and found that Si_5-N14 LNPs predominantly engaged macropinocytosis and lipid raft-mediated endocytosis uptake mechanisms (Supplementary Fig. 25b), while 213-N14 LNPs relied solely on lipid raft-mediated endocytosis (Supplementary Fig. 25d). These findings highlight the critical role of the siloxane domain in facilitating cellular internalization of mRNA.

Due to the larger atomic radius of silicon compared to carbon, the incorporation of a siloxane-based amine head into lipidoids may result in looser packing of lipids in the LNP, which, in turn, could increase the membrane fluidity and promote mRNA transfection efficacy[35] (Fig. 2g). Molecular dynamic simulations showed that the head radius of Si_5-N14 (R = 5.169) was larger than that of 213-N14 (R = 3.197), indicating the potential for increased membrane fluidity after the incorporation of a siloxane moiety (Fig. 2g). To further evaluate membrane fluidity, a fluorescence probe was used to measure reciprocal polarization (1/P), revealing that Si_5-N14 exhibited greater fluidity (1/P = 4.87) compared with 213-N14 (1/P = 2.72) (Fig. 2h). Moreover, membrane fluidity can affect the fusion of endosomal membranes, which is essential for endosomal escape[36]. Confocal laser scanning microscopy imaging showed that Si_5-N14 LNPs exhibited greater endosomal escape than 213-N14 LNPs, as indicated by the greater cytosolic distribution of Cy5-tagged mRNA (red) and lower co-localization between Cy5-tagged mRNA and endosomes (green) in Si_5-N14 LNP-treated cells (Fig. 2i and Supplementary Fig. 26). We then investigated whether the increased endosomal escape facilitated by the Si_5-N14 lipidoid enhances membrane disruption. Results from a haemolysis assay demonstrated that Si_5-N14 LNPs exhibited significantly greater haemolysis than 213-N14 LNPs (Fig. 2j,k). Together, these results support the role of siloxane-incorporated lipidoids for improving LNP cellular internalization and endosomal escape for mRNA delivery.

SiLNP enables tissue-specific mRNA delivery in vivo

The top 50 SiLNPs from in vitro screening were then selected for in vivo FLuc mRNA delivery; however, 14 of these lead candidates exhibited negligible luciferase expression in vivo and were therefore not chosen for further study. Of the remaining 36 SiLNPs that exhibited potent luciferase expression, interestingly, organ-selective mRNA delivery was achieved through altering the siloxane-based amine head and alkyl chain structures (Fig. 3a and Supplementary Table 5). To our knowledge, this is one of the first demonstrations of liver-, lung- and spleen-targeted mRNA delivery from a single lipid library through simple alteration of the lipidoid structure. Siloxane-incorporated lipidoids with epoxide-/ester-based tails mediated SiLNP mRNA delivery primarily to the liver, which is consistent with previous findings featuring non-siloxane structures for hepatic mRNA delivery[30,37]. The top-performing liver SiLNP (Si_6-C14b) exhibited luciferase expression almost exclusively in the liver (~98%) compared with other organs (Fig. 3b).

We also observed that minor structural alterations of siloxane-incorporated lipidoids can substantially alter organ tropism. For instance, substitution of the ester linker with an amine linker on cores such as Si_5-, Si_6- and Si_7- can redirect SiLNP targeting from the liver to the lungs (Fig. 3a), where the Si_5-N14 LNP enabled efficient lung-specific mRNA delivery (~90%) (Fig. 3c). This effect of amide substitution is likely applicable to a broad range of SiLNPs for lung-targeted mRNA delivery, underscoring the importance of varying lipidoid structures to enable organ-tropic mRNA delivery in vivo[10,26].

It has been shown that introducing additional negatively charged phospholipids as a fifth component could assist in splenic mRNA delivery[22,24,25]. However, owing to the poor solubility of these negatively charged phospholipids, their incorporation into LNP formulations is challenging. Engineering ionizable lipids with negatively charged moieties could be another approach to endow LNP formulations with a negative charge, potentially enabling splenic RNA delivery. To this end, a cyclic siloxane structure with multiple reaction sites was designed to attach both a negatively charged sulfonic group and amine head-alkyl tails (Fig. 1d; Si_{12}) to promote spleen tropism in vivo (Fig. 3a). Within this library, Si_{12}-C10 facilitated the most efficient spleen-specific mRNA delivery (Fig. 3d and Supplementary Fig. 20).

After observing this tissue-specific SiLNP mRNA delivery in vivo, we further investigated the influence of these chemical structures on mRNA delivery to the liver, lungs and spleen. First, minor structural alterations of siloxane-incorporated lipidoids can substantially alter organ tropism; we observed that siloxane-incorporated lipidoids with epoxide-/ester-based tails enabled mRNA delivery to the liver, lipidoids with amide tails facilitated mRNA delivery to the lungs, and negatively charged lipidoids facilitated mRNA delivery to the spleen. Second, the importance of tail length was evaluated by analysing the delivery efficacy of siloxane-incorporated lipidoids containing different length tails for each liver-/lung-/spleen-tropic system. A tail length of 12 was found to be optimal for potent mRNA delivery to the liver (Fig. 3e), lungs (Fig. 3f) and spleen (Fig. 3g), while longer or shorter tails generally resulted in lower mRNA delivery. Third, a tail substitution number of 4 contributed to more potent expression in the liver (Fig. 3h), lungs (Fig. 3i) and spleen (Fig. 3j). While there was no obvious correlation between the in vitro and in vivo potencies of the 20 lead SiLNPs (Supplementary Fig. 27), this phenomenon has also been extensively reported by others, emphasizing the importance of evaluating mRNA-LNP delivery in vivo[38].

Si_6-C14b, Si_5-N14 and Si_{12}-C10 were identified as the lead liver-targeting, lung-targeting and spleen-targeting SiLNPs, respectively, as they achieved the most potent and selective mRNA delivery to their respective organs. Afterwards, these selected siloxane-incorporated lipidoids were purified (Supplementary Figs. 12–20) and the resulting SiLNPs were characterized[14,24,25] (Supplementary Fig. 28). Importantly, characterization of these lead lipidoids before in vivo therapeutic studies, including Si_6-C14b and Si_5-N14, showed that purity surpassed

Fig. 2 | Siloxane moiety incorporation improves cellular internalization and endosomal escape. a, Chemical structures and ALog P value of Si_5-N14 and 213-N14 lipidoids. ALog P was predicted from atomic physiochemical properties. **b**, Size, mRNA EE and zeta potential (ζ) of Si_5-N14 and 213-N14 LNPs formulated with Cy5-tagged mRNA. **c**, Representative gating strategy for identifying Cy5-tagged mRNA-LNPs endocytosed by immortalized human lung microvascular endothelial cells (iMVECs). **d**, $Cy5^+$ iMVECs treated with Si_5-N14 and 213-N14 LNPs encapsulating Cy5-tagged mRNA. **e**, Cy5 MFI of iMVECs treated with Si_5-N14 and 213-N14 LNPs at different post-treatment time points. iMVECs were treated with Si_5-N14 and 213-N14 LNPs delivering Cy5-tagged mRNA at an mRNA dose of 200 ng ml^{-1}. **f**, Relative fluorescence intensity versus post-treatment time demonstrated not only faster but also greater endocytosis of Si_5-N14 LNPs than 213-N14 LNPs. Curves were calculated from **e**. **g**, Schematic illustrating differences in lipid packing and the effect on membrane fluidity. The radii of the amine heads for the Si_5-N14 and 213-N14 lipidoids were calculated based on molecular dynamic simulations. Incorporation of the siloxane domain increases the radius of the amine head, which may result in looser lipid packing for improved membrane fluidity for nucleic acid delivery. **h**, Membrane fluidity (1/P) of Si_5-N14 and 213-N14 LNPs was measured by fluorescence polarization. **i**, Representative confocal laser scanning microscopy images of cellular uptake and endosomal escape of Si_5-N14 and 213-N14 LNPs. iMVECs cells were treated with Cy5-tagged mRNA-LNPs (mRNA dose 600 ng ml^{-1}) for 3 h before staining with LysoTracker Green and Hoechst 33342. Scale bars, 50 μm. **j**,**k**, Haemolysis of Si_5-N14 and 213-N14 LNPs at pH 5.5 (**j**) and 7.4 (**k**). Red blood cells (RBCs) were incubated with LNPs at 37 °C for 1 h before the supernatant was transferred into a clear bottom 96-well plate (insert pictures) to determine the adsorption at 540 nm. Statistical significance in **d**, **h**, **j** and **k** was calculated using an unpaired Student's t-test. ****P < 0.0001; ***P < 0.001; *P < 0.05; P > 0.05, not significant. Data are presented as mean ± s.e.m. (**d**,**f**,**h**,**j**,**k**, n = 3 biological independent samples).

https://doi.org/10.1038/s41565-024-01747-6

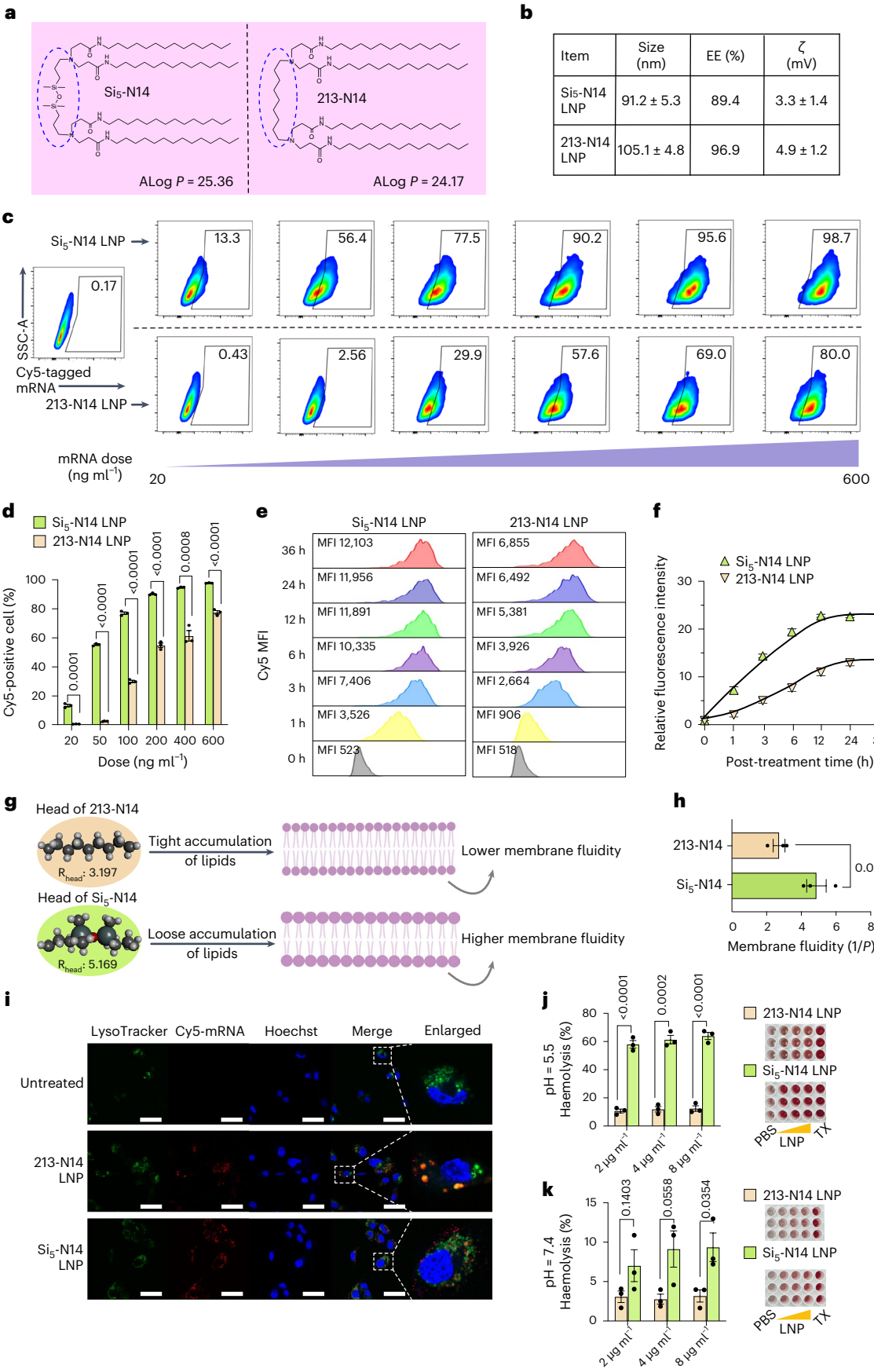

https://doi.org/10.1038/s41565-024-01747-6

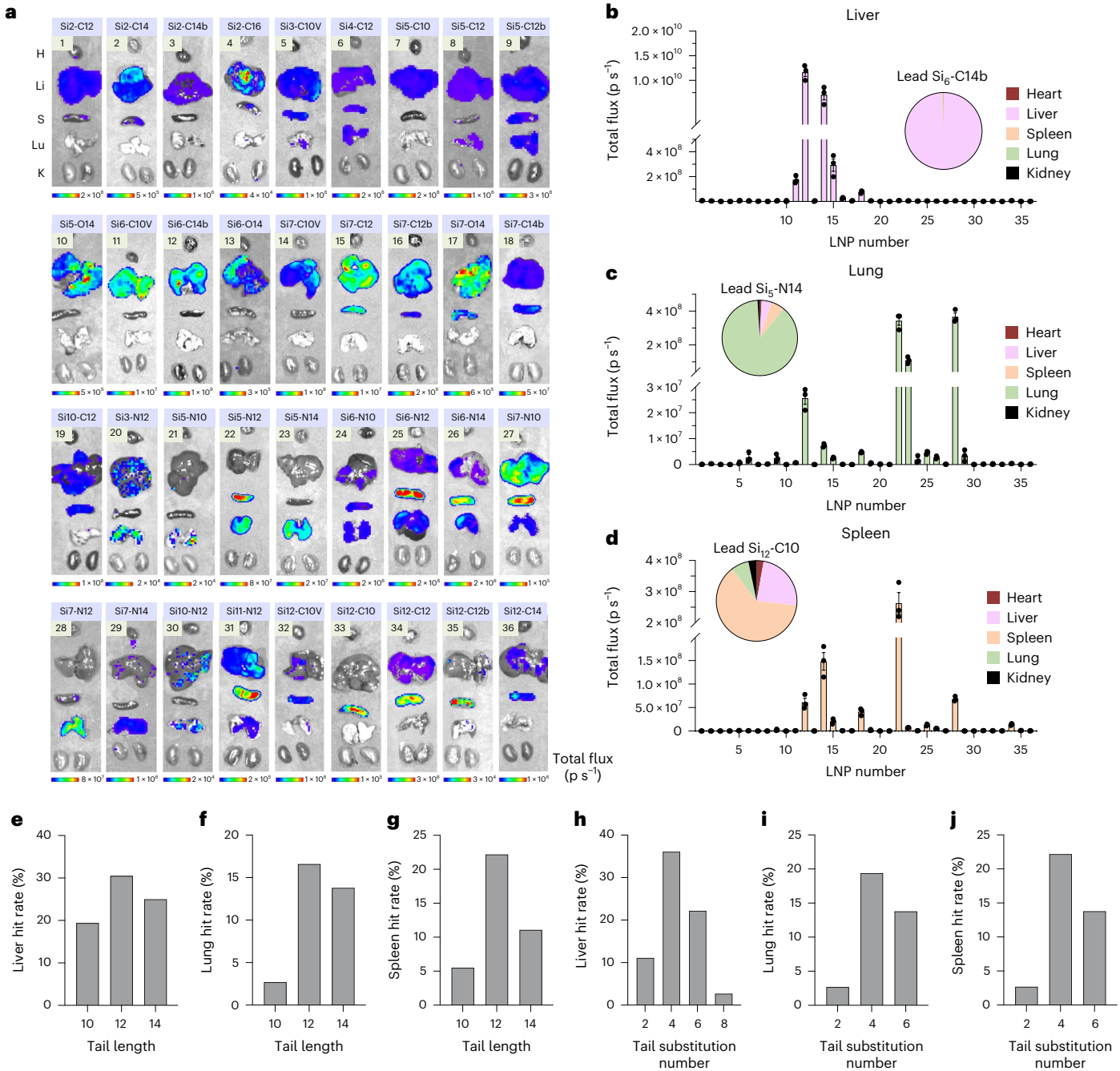

Fig. 3 | In vivo structure–activity studies of siloxane-incorporated lipidoid formulations for mRNA delivery and organ selectivity to the liver, lungs and spleen. a, In vivo evaluation of 36 representative SiLNPs encapsulating FLuc mRNA (dose 0.25 mg kg^{-1}). Representative bioluminescence IVIS images of various organs 6 h after i.v. injection of SiLNPs to C57BL/6J mice. H, heart; Li, liver; S, spleen; Lu, lungs; K, kidneys. **b**–**d**, Quantified luciferase expression in the liver (**b**), lungs (**c**) and spleen (**d**) from the 36 representative SiLNPs. The pie charts in **b**–**d** represent in vivo organ specificity for the top-performing liver-, lung- and spleen-targeted SiLNP formulations. **e**–**j**, Tissue-specific hit rates. Hits were defined as LNPs that enabled luminescence intensity greater than 10^6 p s^{-1} (total flux). Hit rate by tail length for the liver (**e**), lungs (**f**) and spleen (**g**). Hit rate by tail substitution number for the liver (**h**), lungs (**i**) and spleen (**j**). Note that LNP formulations with a tail substitution number of 8 did not generate lungs and spleen hits. Data are presented as mean ± s.e.m. ($n = 3$ mice).

a designated threshold of 90% (Supplementary Figs. 12–19). Moreover, the apparent pK_a of these LNPs was evaluated to determine the potential relationship between pK_a and organ-targeted delivery. The apparent pK_a of the Si$_6$-C14b LNP (6.19) was within the well-established range of 6 to 7 for achieving potent nucleic acid delivery to the liver[9,25] (Supplementary Fig. 28c), while the apparent pK_a of the Si$_5$-N14 LNP (6.92) and Si$_{12}$-C10 LNP (5.84) deviated from the previously reported pK_a measurements of selective organ targeting (SORT) LNPs for mRNA delivery to the lungs and spleen[25] (Supplementary Fig. 28d,e). These discrepancies indicate that the pK_a of LNPs represents only one facet of the complicated landscape governing tissue-specific mRNA delivery.

Liver-specific SiLNP enables CRISPR–Cas9 editing in the liver

After demonstrating tissue-specific mRNA delivery by SiLNPs, we further investigated hepatic mRNA delivery of our top-performing liver-targeted platform. Si$_6$-C14b LNPs mediated 8-fold greater

https://doi.org/10.1038/s41565-024-01747-6

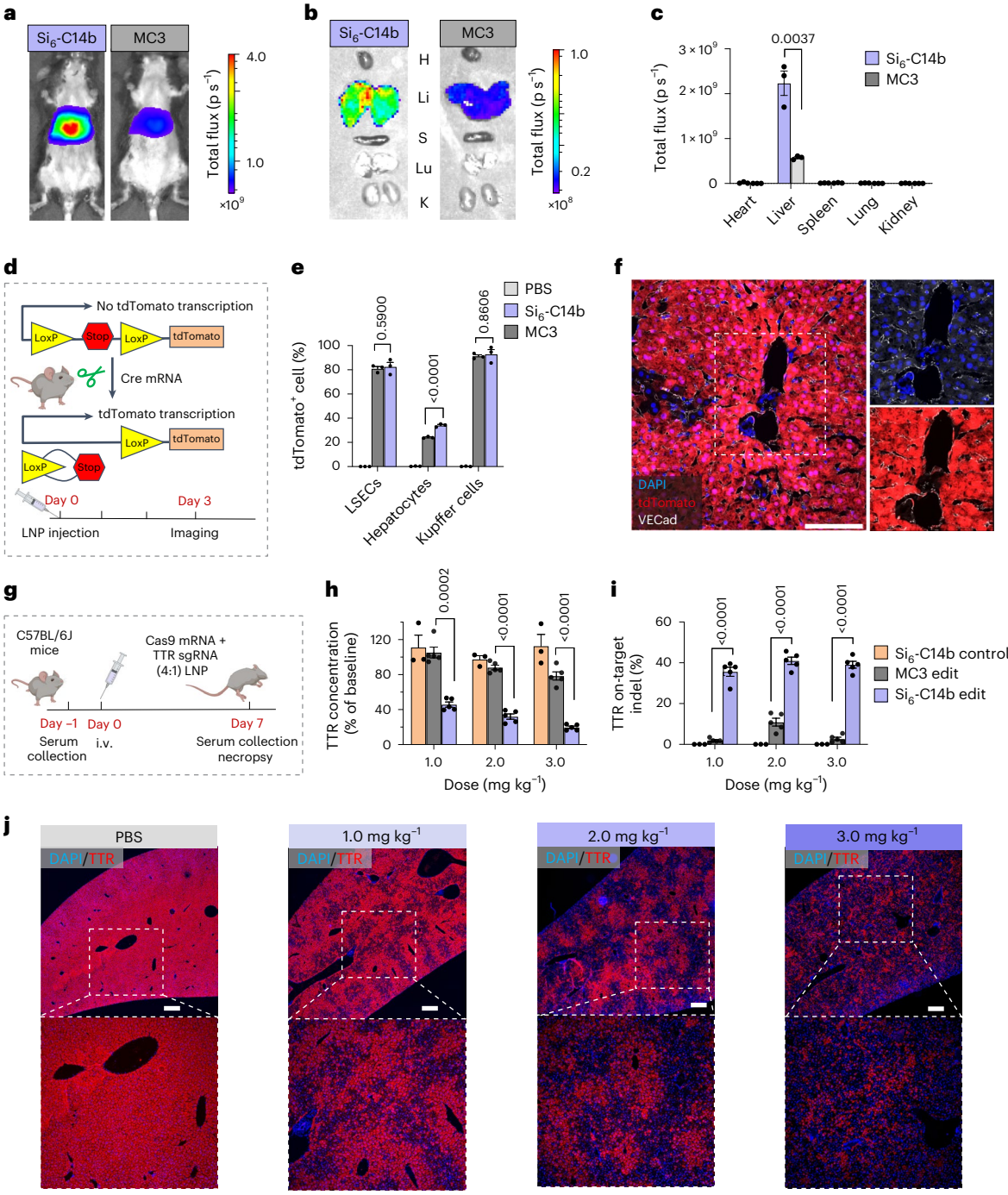

Fig. 4 | Liver-targeted mRNA delivery and CRISPR–Cas9 gene editing by SiLNPs. a, Whole body imaging of luciferase expression by Si_6-C14b and MC3 LNPs 6 h post-injection (FLuc mRNA, 0.15 mg kg^{-1}, $n = 3$ mice). **b**, Ex vivo imaging of luciferase expression in organs from mice depicted in **a** ($n = 3$ mice). H, heart; Li, liver; S, spleen; Lu, lungs; K, kidneys. **c**, Quantification of luciferase expression in organs from **b** ($n = 3$ mice). **d**, Schematic of the Ai14 mouse model, which demonstrates that tdTomato expression is induced upon intracellular Cre mRNA delivery for excision of the stop cassette. **e**, Quantification of the percentage of tdTomato$^+$ cells from PBS-, MC3 LNP- and Si_6-C14b LNP-treated Ai14 mice via flow cytometry (Cre mRNA, 0.3 mg kg^{-1}, $n = 3$ mice). LSECs, liver sinusoidal endothelial cells. **f**, Representative immunostaining of liver histology shows tdTomato fluorescence. DAPI was used for nuclear staining. Vascular endothelial cadherin (VECad) was used for labelling LSECs. Scale bar, 100 µm. **g**, Schematic representation of CRISPR–Cas9 gene editing of transthyretin amyloidosis (*TTR*). C57BL/6J mice were systemically injected with a single dose of LNPs co-formulated with Cas9 mRNA and *TTR* sgRNA (wt/wt, 4/1). LNPs co-delivering Cas9 mRNA/scrambled sgRNA control were used as negative controls. Serum was collected 1 day before and 7 days post-injection. **h**, Serum *TTR* concentration in mice following treatment from **g**. **i**, *TTR* on-target indel frequency in the liver following treatment from **g** (**h**,**i**, $n = 3$ mice for the Si_6-C14b LNP control group; $n = 5$ mice for the MC3 and Si_6-C14b LNP editing group). **j**, Reduction of *TTR* transcript was visualized by in situ hybridization of liver sections from mice treated with PBS or Si_6-C14b LNPs encapsulating Cas9 mRNA and *TTR* sgRNA. Scale bars, 200 µm. Statistical significance in **c** was calculated using an unpaired Student's *t*-test. Statistical significance in **e**, **h** and **i** was calculated using one-way ANOVA, followed by Dunnett's multiple comparison test. $^{****}P < 0.0001$; $^{***}P < 0.001$; $^{**}P < 0.01$. Data are presented as mean ± s.e.m.

luciferase expression in the liver compared with the MC3 LNP, a gold standard LNP formulation (Fig. 4a–c). To further characterize the transfection of liver cell types, the activatable Cre-LoxP mouse (Ai14) model that expresses Lox-stop-Lox tdTomato was used[39]. In this model, upon intracellular delivery of Cre-recombinase mRNA (Cre mRNA), the translated Cre protein deletes the stop cassette and activates tdTomato expression only in transfected cells (Fig. 4d). Following administration of Cre mRNA, Si_6-C14b LNPs mediated mRNA delivery to ~35% of hepatocytes, ~70% of liver sinusoidal endothelial cells (LSECs) and ~82% of Kupffer cells (Fig. 4e,f and Supplementary Figs. 29 and 30), exhibiting higher delivery efficacy than MC3 LNPs.

We then evaluated CRISPR–Cas9 genome editing in a therapeutic mouse model through the delivery of mRNA SiLNPs to the liver. Si_6-C14b LNPs formulated with Cas9 mRNA and sgRNA were systemically administered at doses of 1.0 mg kg^{-1}, 2.0 mg kg^{-1} and 3.0 mg kg^{-1} of total RNA (mRNA/sgRNA, 4/1, wt/wt) targeting the mouse *TTR* gene in the liver (Supplementary Table 6). We quantified gene editing by examining serum *TTR* protein concentration and on-target editing through DNA sequencing 7 days post-injection (Fig. 4g). MC3 LNP co-delivering Cas9 mRNA/*TTR* sgRNA was included as a positive control. Si_6-C14b LNPs mediated greater knockout of serum *TTR* than MC3 LNPs (Fig. 4h). To validate these results, the frequency of on-target editing of the *TTR* gene was also investigated (Fig. 4i). Given the branched tail structure of the Si_6-C14b lipidoid, we also utilized a representative branched lipidoid, 306Oi10, to compare to the gene editing efficacy of our platform[40]. Si_6-C14b LNP exhibited enhanced TTR editing when compared with the 306Oi10 LNP (Supplementary Fig. 31). In situ hybridization (ISH) analysis of liver sections further confirmed dose-dependent knockout of the *TTR* transcript (Fig. 4j).

Next, we investigated the kinetics of *TTR* editing by measuring on-target indel sequencing at 6 h, 24 h and 7 days post-injection of SiLNPs. Editing was detected as soon as 6 h post-injection, and editing efficacy increased at later post-injection time points (Supplementary Fig. 32). Importantly, editing lasted for at least 56 days after a single administration dose (Supplementary Fig. 33). Analysis of liver enzymes and kidney toxicity demonstrated negligible in vivo toxicity of Si_6-C14b LNPs (Extended Data Fig. 2a–d). Collectively, these results suggest the potential of SiLNP formulations for liver-specific protein replacement and gene editing therapies.

Lung-specific SiLNP for CRISPR–Cas9 editing in the lungs

When the structure of siloxane-incorporated lipidoids was altered by incorporating two silicon atoms, two tertiary amines and four amide-bond featured C14 alkyl chains (Supplementary Fig. 18), the resulting Si_5-N14 LNPs exhibited lung-specific mRNA delivery (Fig. 5a–c). We then studied the biodistribution of Si_5-N14 LNP to further understand the observed lung-tropic protein expression. Si_5-N14 lipidoids were extracted from tissues (liver, spleen and lungs) and quantified through mass spectrometry. While luciferase expression was observed primarily in the lungs (Fig. 5b), Si_5-N14 was detected both in the lungs and liver, accompanied by a discernible fraction in the spleen (Supplementary Fig. 34). This demonstrates a weak correlation between LNP organ accumulation, cellular uptake and protein expression, which is a phenomenon observed by others[26]. An additional pharmacokinetics study of Si_5-N14 in these organs showed a clearance profile of Si_5-N14 lipidoids (Supplementary Fig. 34).

To explore the potential mechanism of lung targeting by Si_5-N14 LNPs, we identified and quantified the top 20 proteins bound to Si_5-N14 LNPs following incubation in plasma (Fig. 5d and Supplementary Table 7). Among them, vitronectin (Vtn) was identified as the most highly enriched protein at an average abundance of 16.1%, which is a 320-fold enrichment compared with native mouse plasma (Fig. 5e). Vtn can bind its cognate receptor, $\alpha_v\beta_3$ integrin, which is highly expressed by the pulmonary endothelium, providing a plausible explanation for lung targeting with our Si_5-N14 LNP[25,41]. In addition, the limited binding of apolipoprotein E (ApoE) (~0.3%) could also promote extrahepatic mRNA delivery compared with previously reported liver-tropic mRNA delivery systems[9,25]. Together, these findings suggest that proteins with different molecular weights (M_w) and isoelectric points (pI) in the corona of Si_5-N14 LNPs may collectively promote mRNA delivery to the lungs (Fig. 5f).

To characterize transfected cell types in the lungs, we delivered Cre mRNA with Si_5-N14 LNPs in the Ai14 mouse model (Fig. 5g) and observed high specificity for lung endothelial cells (~88%) (Fig. 5h–j and Supplementary Fig. 35). Immunostaining of the lungs showed that Si_5-N14 LNPs mainly transfected the capillary endothelial cells of the microvasculature in the lungs, with low transfection of the large vessels and airway (Fig. 5k and Supplementary Fig. 36).

Next, we assessed co-delivery of Cas9 mRNA and sgRNA with Si_5-N14 LNPs to enable CRISPR–Cas9 genome editing in the lungs. Si_5-N14 LNPs encapsulating Cas9 mRNA and GFP sgRNA with different weight ratios (4/1, 3/1, 2/1 and 1/1) were initially formulated to investigate the efficacy of GFP knockout in GFP-HepG2 cells (Supplementary Table 6 and Supplementary Fig. 37). In vitro gene editing efficacy was highly dependent on the Cas9 mRNA/GFP sgRNA ratio, indicating that a weight ratio of 4/1 enabled the most effective GFP knockout in GFP-HepG2 cells (Supplementary Fig. 37). Si_5-N14 LNPs edited over 80% of GFP-HepG2 cells, as further indicated by fluorescence imaging (Supplementary Fig. 38). Si_5-N14 LNPs co-delivering Cas9 mRNA and GFP sgRNA (4/1) were then formulated to assess in vivo CRISPR–Cas9 gene editing in a transgenic GFP mouse model. Gene editing in the lungs has been reported to benefit from repeated dosing owing to its high rate of cell turnover[42]; thus, Si_5-N14 LNPs co-delivering Cas9 mRNA and GFP sgRNA were systemically administered once per day for a total of 4 days, each at a dose of 0.5 mg kg^{-1}. Lung tissues were then dissected for further evaluation of GFP knockout 7 days following the final injection (Fig. 5l). Nearly ~20% of endothelial cells and ~8% of epithelial cells in the lungs

Fig. 5 | Lung-targeted mRNA delivery and CRISPR–Cas9 gene editing by SiLNPs. a, Characterization of the Si_5-N14 LNP formulated with FLuc mRNA. **b**, Luciferase expression imaging from Si_5-N14 LNPs 6 h post-injection (FLuc mRNA, 0.3 mg kg^{-1}). H, heart; Li, liver; S, spleen; Lu, lungs; K, kidneys. **c**, Quantification of luciferase expression in organs from mice depicted in **b**. **d**, Schematic representation of the interaction of Si_5-N14 LNPs with proteins in blood vessels. **e**, Quantification of the top five proteins in the corona of the Si_5-N14 LNP. Vtn, vitronectin; Alb, serum albumin; Apob, apolipoprotein B-100; C3, complement C3; Hbb-b1, haemoglobin subunit beta-1. **f**, The top 20 most abundant corona proteins were categorized by molecular weight and isoelectric point. **g**, Ai14 mice were treated with Si_5-N14 LNPs formulated with Cre mRNA for 3 days before analysis (Cre mRNA, 0.3 mg kg^{-1}). **h**, Representative gating strategy to identify tdTomato$^+$ ECs (CD45$^-$/CD31$^+$/tdTomato$^+$). **i**, Percentage of tdTomato$^+$ cells in the lung by flow cytometry. **j**, Distribution of tdTomato$^+$ cells in each cell type. **k**, Representative immunostaining demonstrating substantial co-localization of tdTomato$^+$ cells and an EC marker, platelet endothelial cell adhesion molecule 1 (PECAM1). DAPI was used for nuclear staining. Scale bars, 50 µm. **l**, Schematic demonstration of in vivo gene editing in the lungs of transgenic GFP mice treated with Si_5-N14 LNPs co-formulated with Cas9 mRNA and GFP sgRNA (4 injections, RNA dose 0.5 mg kg^{-1} per injection). PBS or Si_5-N14 LNPs co-delivering Cas9 mRNA/scrambled sgRNA were used as negative controls. **m**, Quantification of the percentage of GFP$^-$ cells in the lungs by flow cytometry. **n**, Representative immunostaining showed GFP knockout in lung ECs. DAPI was used for staining nuclei. PECAM1 was used for labelling ECs. ERG was used for staining EC nuclei. Scale bars, 50 µm. **o**, RT–qPCR analysis of GFP in sorted ECs. Statistical significance in **i** was calculated using an unpaired Student's *t*-test. Statistical significance in **m** and **o** was calculated using one-way ANOVA, followed by Dunnett's multiple comparison test. $^{****}P < 0.0001$; $^{***}P < 0.001$; $^{**}P < 0.01$; $^{*}P < 0.05$. Data are presented as mean ± s.e.m. ($n = 3$ mice).

https://doi.org/10.1038/s41565-024-01747-6

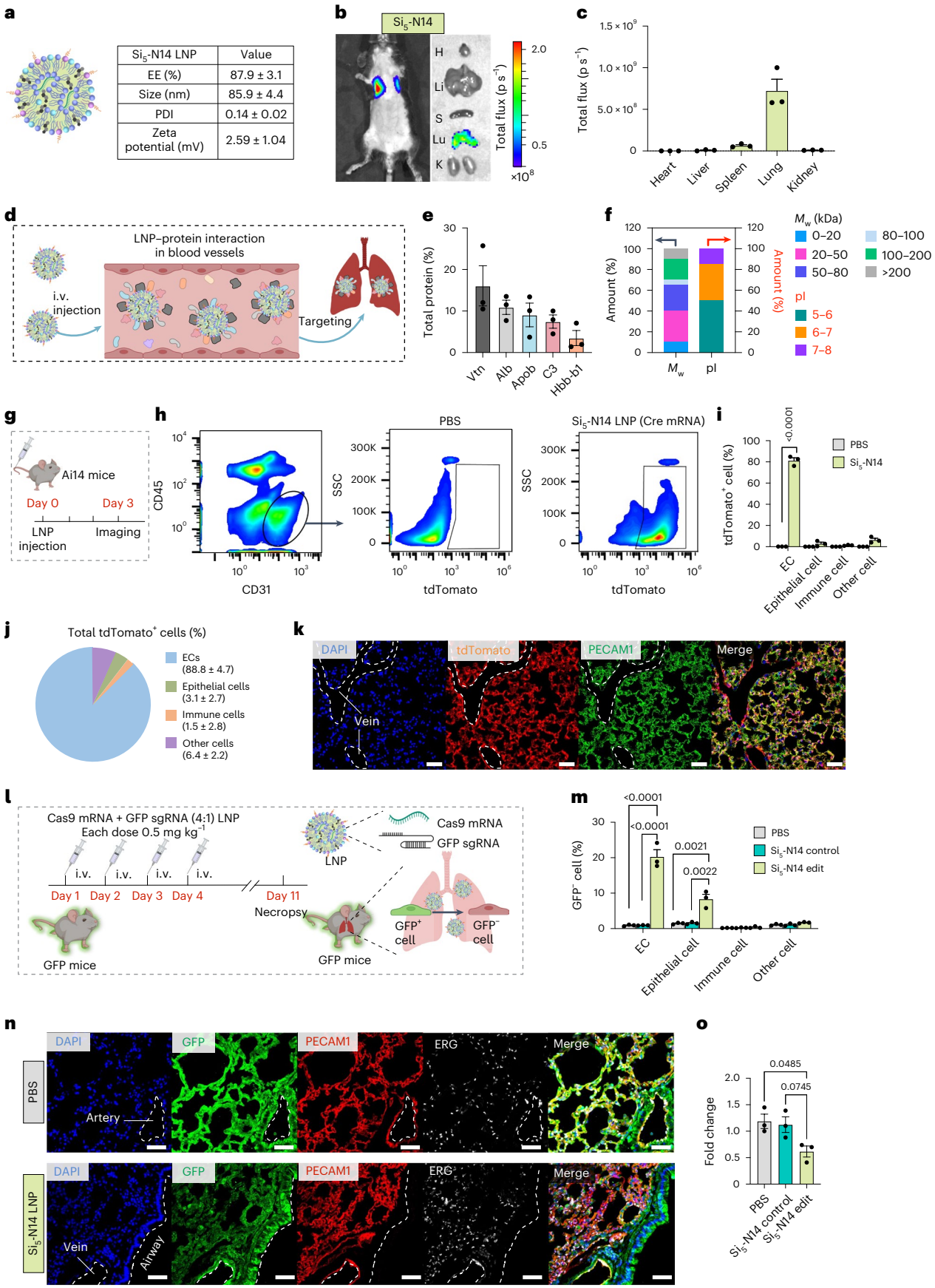

https://doi.org/10.1038/s41565-024-01747-6

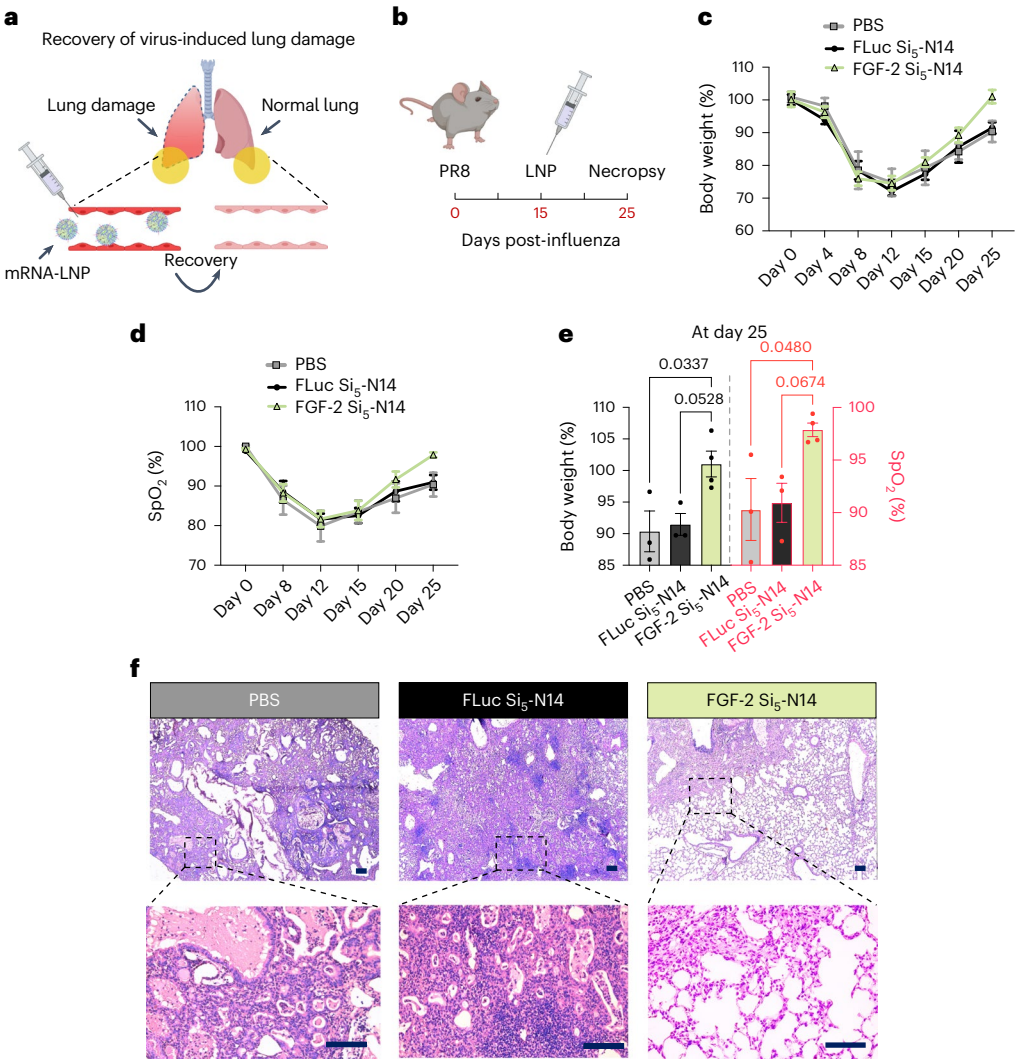

Fig. 6 | Lung-targeted SiLNPs for efficient vascular repair. a, Schematic illustration of endothelial repair for lung recovery through LNP-mediated delivery of mRNA encoding angiogenic factors in a viral infection lung damage model. **b**, Schematic timeline for LNP administration and sampling. Influenza virus A/H1N1/PR/8 was administered intranasally at 50–60 TCID50 units to female C57BL/6J mice. After injection, mice were treated with control (PBS or FLuc mRNA Si_5-N14 LNPs, $n = 3$ mice) or FGF-2 mRNA Si_5-N14 LNPs (0.5 mg kg^{-1}, $n = 4$ mice) on day 15, and lungs were collected on day 25. Dexamethasone-21-phosphate (DEX) was administered intraperitoneally (i.p., 2 mg kg^{-1}) to mice 30 min before LNP administration. **c**,**d**, Time course changes in weight loss (**c**) and capillary oxygen saturation (**d**) were observed in virus-infected C57BL/6J mice treated with either control (PBS or FLuc mRNA Si_5-N14 LNPs) or FGF-2 mRNA Si_5-N14 LNPs. **e**, Analysis of body weight and blood oxygen levels on day 25 after treatment with either control (PBS or FLuc mRNA Si_5-N14 LNPs) or FGF-2 mRNA Si_5-N14 LNPs to lung-damaged mice. **f**, Histological changes in the lungs of mice after receiving control (PBS or FLuc mRNA Si_5-N14 LNPs) or FGF-2 mRNA Si_5-N14 LNPs 25 days after infection. White areas in H&E stained sections are pulmonary alveoli, airway and large vessels, while dark spots represent the nuclei. Accumulated dark regions indicate large amounts of immune cell infiltration, leading to damaged inflammatory areas. Scale bars, 100 μm. Statistical significance in **e** was calculated using one-way ANOVA, followed by Dunnett's multiple comparison test. $^*P < 0.05$; $P > 0.05$, not significant. Data are presented as mean ± s.e.m.

were edited (Fig. 5m and Supplementary Fig. 39) and immunostaining of the lungs showed a marked decrease in GFP signal in endothelial cells of the microvasculature (Fig. 5n and Supplementary Fig. 40). We then sorted endothelial cells from the lungs to evaluate the editing efficacy by real-time quantitative PCR (RT–qPCR), which demonstrated that GFP expression significantly decreased in sorted endothelial cells after SiLNP-mediated CRISPR–Cas9 editing (Fig. 5o). Subsequently, we measured the levels of pro-inflammatory cytokines in both serum and bronchoalveolar lavage fluid (BALF) to assess if repeated dosing of Si_5-N14 LNPs elicited an immune response. We observed that the pro-inflammatory cytokines were upregulated 6 h post-repeat injection, but these cytokines returned to baseline after 48 h (Supplementary Fig. 41), demonstrating that repeated dosing of Si_5-N14 LNPs did not induce a long-term systemic inflammatory response.

To further show the therapeutic editing potential of Si_5-N14 LNPs, we established a classical Lewis lung carcinoma (LLC) tumour model and demonstrated knockout of vascular endothelial growth factor receptor 2 (VEGFR2) expression in lung endothelial cells for antiangiogenic cancer therapy[43,44]. Mice bearing LLC tumours were systemically treated with Si_5-N14 LNPs encapsulating Cas9 mRNA/VEGFR2 sgRNA, while Cas9 mRNA/scramble sgRNA-loaded Si_5-N14 LNPs and PBS-treated groups were used as controls. LLC-bearing mice treated with Si_5-N14 LNPs encapsulating Cas9 mRNA/VEGFR2 sgRNA exhibited substantial anti-tumour efficacy, with decreased expression of VEGFR2 and notable reduction in lung tumour burden following CRISPR–Cas9 editing (Supplementary Fig. 42). These results collectively demonstrate that Si_5-N14 LNPs enable lung-targeted mRNA delivery and lung-specific genome editing in lung endothelial cells.

SiLNP enables endothelial repair for lung regeneration

Owing to the potent pulmonary endothelium targeting of Si_5-N14 LNPs, we then evaluated the therapeutic potential of Si_5-N14 LNPs for treating vascular-related diseases in the lungs[45]. We established a viral infection lung vasculature damage model and investigated whether endothelial overexpression of FGF-2 would accelerate the recovery of lung function[46,47] (Fig. 6a,b). Successful FGF-2 expression was confirmed by collecting serum from mice treated with Si_5-N14 LNPs encapsulating FGF-2 mRNA (Supplementary Fig. 43). To avoid potential inflammation exacerbation, dexamethasone was injected intraperitoneally into mice before administering Si_5-N14 mRNA-LNPs for lung function recovery[45]. FGF-2 protein was detected in the BALF of virus-infected mice treated with the Si_5-N14 LNP encapsulating FGF-2 mRNA (Supplementary Fig. 44), which may have leaked across the damaged lung endothelium induced by viral infection. In addition, treatment with FGF-2 mRNA-LNPs improved lung function, as evidenced by improved recovery of body weight and increased blood oxygen levels compared with the LNP control groups (Fig. 6c–e). Histopathological evaluation of the lungs showed less inflammation and improved remodelling with FGF-2 mRNA Si_5-N14 LNP treatment compared with respective controls, as evidenced by less damage of alveolar architecture and limited leukocyte infiltration (Fig. 6f). Furthermore, decreased lung function recovery was observed without pretreatment with dexamethasone (Supplementary Fig. 45). In direct comparison to the well-characterized SORT-DOTAP and 7C1 LNPs[22,48], Si_5-N14 LNPs demonstrated minimal toxicity, as indicated by blood chemistry assessment, immune cell infiltration in the lung and histopathological evaluation (Supplementary Fig. 46). Collectively, these results indicate that delivery of FGF-2 mRNA to the lung endothelium via Si_5-N14 LNPs enhances vascular repair, demonstrating the potential of SiLNPs for targeted delivery of regenerative therapeutics to the lungs.

In addition to liver- and lung-targeted mRNA delivery, the spleen-targeted Si_{12}-C10 LNP demonstrated potential for editing splenic dendritic cells and macrophages (Supplementary Fig. 47). These top-performing tissue-targeted SiLNPs adsorb various proteins on their surface, which may help facilitate their organ-specific targeting capabilities (Supplementary Tables 7–9 and Supplementary Fig. 48). Furthermore, siloxane domain incorporation improved the stability and safety of SiLNPs (Supplementary Figs. 49 and 50); however, unlike previous works that report potential adjuvanticity of siloxane moieties[49], a representative siloxane-incorporated lipidoid did not exhibit adjuvant activity in a dendritic cell line (Supplementary Fig. 51).

Conclusion

In summary, we report a combinatorial design approach to synthesize a library of 252 siloxane-incorporated lipidoids to formulate SiLNPs for tissue-specific mRNA delivery. The incorporation of a siloxane moiety into lipidoids enhances endocytosis of mRNA-LNPs as well as LNP endosomal escape. Moreover, structural alteration of siloxane-incorporated lipidoids substantially modulates the organ tropism of mRNA-LNPs. Liver-specific SiLNPs delivering gene editing cargo demonstrated robust editing at the *TTR* locus in the liver of wild-type C57BL/6J mice. In addition, lung-specific SiLNPs delivering gene editing cargo efficiently edited lung endothelial cells in a transgenic GFP mouse model and a therapeutic LLC mouse model. The integration of siloxane domains resulted in improved stability of mRNA-LNPs, concomitant with limited in vivo toxicity. Furthermore, lung-targeted SiLNPs delivering FGF-2 mRNA improved vascular endothelial recovery in a viral infection lung vascular damage model. These findings highlight the potential for developing ionizable lipid libraries for potent, tissue-specific mRNA delivery for protein replacement and gene editing therapies.

Online content

Any methods, additional references, Nature Portfolio reporting summaries, source data, extended data, supplementary information, acknowledgements, peer review information; details of author contributions and competing interests; and statements of data and code availability are available at https://doi.org/10.1038/s41565-024-01747-6.

References

1. Chaudhary, N., Weissman, D. & Whitehead, K. A. mRNA vaccines for infectious diseases: principles, delivery and clinical translation. *Nat. Rev. Drug Discov.* **20**, 817 (2021).
2. Pardi, N., Hogan, M. J., Porter, F. W. & Weissman, D. mRNA vaccines—a new era in vaccinology. *Nat. Rev. Drug Discov.* **17**, 261 (2018).
3. Sahin, U., Karikó, K. & Türeci, O. mRNA-based therapeutics—developing a new class of drugs. *Nat. Rev. Drug Discov.* **13**, 759 (2014).
4. Mendes, B. B. et al. Nanodelivery of nucleic acids. *Nat. Rev. Methods Prim.* **2**, 24 (2022).
5. Pastor, F. et al. An RNA toolbox for cancer immunotherapy. *Nat. Rev. Drug Discov.* **17**, 751 (2018).
6. Miao, L., Zhang, Y. & Huang, L. mRNA vaccine for cancer immunotherapy. *Mol. Cancer* **20**, 41 (2021).
7. Zhang, H., Zhang, Y. & Yin, H. Genome editing with mRNA encoding ZFN, TALEN, and Cas9. *Mol. Ther.* **27**, 735 (2019).
8. Yin, H., Kauffman, K. J. & Anderson, D. G. Delivery technologies for genome editing. *Nat. Rev. Drug Discov.* **16**, 387 (2017).
9. Akinc, A. et al. The Onpattro story and the clinical translation of nanomedicines containing nucleic acid-based drugs. *Nat. Nanotechnol.* **14**, 1084 (2019).
10. Hou, X., Zaks, T., Langer, R. & Dong, Y. Lipid nanoparticles for mRNA delivery. *Nat. Rev. Mater.* **6**, 1078 (2021).
11. Hajj, K. A. & Whitehead, K. A. Tools for translation: non-viral materials for therapeutic mRNA delivery. *Nat. Rev. Mater.* **2**, 17056 (2017).
12. Finn, J. D. et al. A single administration of CRISPR/Cas9 lipid nanoparticles achieves robust and persistent in vivo genome editing. *Cell Rep.* **22**, 2227 (2018).
13. Gillmore, J. D. et al. CRISPR-Cas9 in vivo gene editing for transthyretin amyloidosis. *N. Engl. J. Med.* **385**, 493 (2021).
14. Whitehead, K. A. et al. Degradable lipid nanoparticles with predictable in vivo siRNA delivery activity. *Nat. Commun.* **5**, 4277 (2014).
15. Qiu, M., Li, Y., Bloomer, H. & Xu, Q. Developing biodegradable lipid nanoparticles for intracellular mRNA delivery and genome editing. *Acc. Chem. Res.* **54**, 4001 (2021).
16. Hou, X. et al. Vitamin lipid nanoparticles enable adoptive macrophage transfer for the treatment of multidrug-resistant bacterial sepsis. *Nat. Nanotechnol.* **15**, 41 (2020).
17. Zhao, X. et al. Imidazole-based synthetic lipidoids for in vivo mRNA delivery into primary T lymphocytes. *Angew. Chem. Int. Ed.* **59**, 20083 (2020).
18. Zhou, K. et al. Modular degradable dendrimers enable small RNAs to extend survival in an aggressive liver cancer model. *Proc. Natl Acad. Sci. USA* **113**, 520 (2016).
19. Miao, L. et al. Delivery of mRNA vaccines with heterocyclic lipids increases anti-tumor efficacy by STING-mediated immune cell activation. *Nat. Biotechnol.* **37**, 1174 (2019).
20. Xue, L. et al. Rational design of bisphosphonate lipid-like materials for mRNA delivery to the bone microenvironment. *J. Am. Chem. Soc.* **144**, 9926 (2022).
21. Li, W. et al. Biomimetic nanoparticles deliver mRNAs encoding costimulatory receptors and enhance T cell mediated cancer immunotherapy. *Nat. Commun.* **12**, 7264 (2021).

22. Cheng, Q. et al. Selective organ targeting (SORT) nanoparticles for tissue-specific mRNA delivery and CRISPR-Cas gene editing. *Nat. Nanotechnol.* **15**, 313 (2020).
23. Kulkarni, J. A., Witzigmann, D., Chen, S., Cullis, P. R. & van der Meel, R. Lipid nanoparticle technology for clinical translation of siRNA therapeutics. *Acc. Chem. Res.* **52**, 2435 (2019).
24. Liu, S. et al. Membrane-destabilizing ionizable phospholipids for organ-selective mRNA delivery and CRISPR-Cas gene editing. *Nat. Mater.* **20**, 701 (2021).
25. Dilliard, S. A., Cheng, Q. & Siegwart, D. J. On the mechanism of tissue-specific mRNA delivery by selective organ targeting nanoparticles. *Proc. Natl Acad. Sci. USA* **118**, e2109256118 (2021).
26. Qiu, M. et al. Lung-selective mRNA delivery of synthetic lipid nanoparticles for the treatment of pulmonary lymphangioleiomyomatosis. *Proc. Natl Acad. Sci. USA* **119**, e2116271119 (2022).
27. Shahbazi, M. A., Herranz, B. & Santos, H. A. Nanostructured porous Si-based nanoparticles for targeted drug delivery. *Biomatter* **2**, 296 (2012).
28. Tang, F., Li, L. & Chen, D. Mesoporous silica nanoparticles: synthesis, biocompatibility and drug delivery. *Adv. Mater.* **24**, 1504 (2012).
29. Frampton, M. B. et al. Exploring the utility of hybrid siloxane-phosphocholine (SiPC) liposomes as drug delivery vehicles. *RSC Adv.* **11**, 13014 (2021).
30. Semple, S. C. et al. Rational design of cationic lipids for siRNA delivery. *Nat. Biotechnol.* **28**, 172 (2010).
31. Zhu, Y. et al. Multi-step screening of DNA/lipid nanoparticles and co-delivery with siRNA to enhance and prolong gene expression. *Nat. Commun.* **13**, 4282 (2022).
32. Hu, B. et al. Thermostable ionizable lipid-like nanoparticles (iLAND) for RNAi treatment of hyperlipidemia. *Sci. Adv.* **8**, eabm1418 (2022).
33. Ni, X., Kelly, S. S., Xu, S. & Xian, M. The path to controlled delivery of reactive sulfur species. *Acc. Chem. Res.* **54**, 3968 (2021).
34. Behzadi, S. et al. Cellular uptake of nanoparticles: journey inside the cell. *Chem. Soc. Rev.* **46**, 4218 (2017).
35. Wei, Y. et al. A cationic lipid with advanced membrane fusion performance for pDNA and mRNA delivery. *J. Mater. Chem. B* **11**, 2095 (2023).
36. Tokudome, Y. et al. Preparation and characterization of ceramide-based liposomes with high fusion activity and high membrane fluidity. *Colloids Surf. B* **73**, 92 (2009).
37. Akinc, A. et al. A combinatorial library of lipid-like materials for delivery of RNAi therapeutics. *Nat. Biotechnol.* **26**, 561 (2008).
38. Paunovska, K. et al. A direct comparison of in vitro and in vivo nucleic acid delivery mediated by hundreds of nanoparticles reveals a weak correlation. *Nano Lett.* **18**, 2148 (2018).
39. Nagy, A. Cre recombinase: the universal reagent for genome tailoring. *Genesis* **26**, 99 (2000).
40. Hajj, K. A. et al. A potent branched-tail lipid nanoparticle enables multiplexed mRNA delivery and gene editing in vivo. *Nano Lett.* **20**, 5167 (2020).
41. Singh, B., Fu, C. & Bhattacharya, J. Vascular expression of the $\alpha_v\beta_3$-integrin in lung and other organs. *Am. J. Physiol. Lung Cell. Mol. Physiol.* **278**, L217 (2000).
42. Alton, E. et al. Toxicology study assessing efficacy and safety of repeated administration of lipid/DNA complexes to mouse lung. *Gene Ther.* **21**, 89 (2014).
43. Ebos, J. & Kerbel, R. S. Antiangiogenic therapy: impact on invasion, disease progression, and metastasis. *Nat. Rev. Clin. Oncol.* **8**, 210 (2011).
44. Xue, L. et al. High-throughput barcoding of nanoparticles identifies cationic, degradable lipid-like materials for mRNA delivery to the lungs in female preclinical models. *Nat. Commun.* **15**, 1884 (2024).
45. Zhao, G. et al. TGF-βR2 signaling coordinates pulmonary vascular repair after viral injury in mice and human tissue. *Sci. Trans. Med.* **16**, eadg6229 (2024).
46. Jia, T. et al. FGF-2 promotes angiogenesis through a SRSF1/SRSF3/SRPK1-dependent axis that controls VEGFR1 splicing in endothelial cells. *BMC Biol.* **19**, 173 (2021).
47. Cao, R. et al. Comparative evaluation of FGF-2-, VEGF-A-, and VEGF-C-induced angiogenesis, lymphangiogenesis, vascular fenestrations, and permeability. *Circ. Res.* **94**, 664 (2004).
48. Dahlman, J. E. et al. In vivo endothelial siRNA delivery using polymeric nanoparticles with low molecular weight. *Nat. Nanotechnol.* **9**, 648 (2014).
49. McDermott, M. R., Brook, M. A. & Bartzoka, V. Adjuvancy effect of different types of silicone gel. *J. Biomed. Mater. Res.* **46**, 132 (1999).

[1]Department of Bioengineering, University of Pennsylvania, Philadelphia, Pennsylvania, USA. [2]Department of Biomedical Sciences, School of Veterinary Medicine, University of Pennsylvania, Philadelphia, Pennsylvania, USA. [3]Yangtze Delta Region Institute (Huzhou), University of Electronic Science and Technology of China, Huzhou, China. [4]Gene Therapy Program, Perelman School of Medicine, University of Pennsylvania, Philadelphia, Pennsylvania, USA. [5]Institute of Fundamental and Frontier Sciences, University of Electronic Science and Technology of China, Chengdu, China. [6]Department of Materials Science and Engineering, University of Delaware, Newark, Delaware, USA. [7]Department of Medicine, University of Pennsylvania, Philadelphia, Pennsylvania, USA. [8]Penn Institute for RNA Innovation, Perelman School of Medicine, University of Pennsylvania, Philadelphia, Pennsylvania, USA. [9]Department of Bioengineering, Temple University, Philadelphia, Pennsylvania, USA. [10]Abramson Cancer Center, Perelman School of Medicine, University of Pennsylvania, Philadelphia, Pennsylvania, USA. [11]Institute for Immunology, Perelman School of Medicine, University of Pennsylvania, Philadelphia, Pennsylvania, USA. [12]Cardiovascular Institute, Perelman School of Medicine, University of Pennsylvania, Philadelphia, Pennsylvania, USA. [13]Institute for Regenerative Medicine, Perelman School of Medicine, University of Pennsylvania, Philadelphia, Pennsylvania, USA. [14]These authors contributed equally: Lulu Xue, Gan Zhao, Ningqiang Gong. ✉e-mail: mjmitch@seas.upenn.edu

Methods

Biological reagents

Luciferase and FGF-2 mRNA were provided by Drew Weissman. CleanCap Cre mRNA (catalogue number L-7211), CleanCap OVA mRNA (catalogue number L-7210) and CleanCap Cas9 mRNA (catalogue number L-7206) were purchased from TriLink Biotechnologies. GFP sgRNA were obtained from Axolabs GmbH. VEGFR2 sgRNA were obtained from Synthego. Luciferase 1000 Assay System (ref. E4550) was purchased from Promega Corporation. Alanine transaminase (ALT) colorimetric activity assay kit (item 700260) and aspartate aminotransferase (AST) colorimetric activity assay kit (item 701640) for liver toxicity markers were purchased from Cayman Chemical. Urea assay kit (BUN, item ab83362), triglyceride assay kit (item ab65336) and creatinine assay kit (item ab65340) for kidney toxicity markers were purchased from Abcam. Prealbumin ELISA kit (catalogue number OKIA00111) for mouse *TTR* measurement was purchased from Aviva Systems Biology. ISH kit for *TTR* mRNA (LS 2.5 Probe, Mm-Ttr, catalogue number 424178) was purchased from ACD Bio. Antibodies for flow cytometry including anti-mouse CD31 antibody (AF488, catalogue number 102514; PE, catalogue number 102508), CD45 antibody (BV421, catalogue number 103134), F4/80 antibody (BV421, catalogue number 123137; AF647, catalogue number 123122), CD3 antibody (AF700, catalogue number 100216), CD19 antibody (AF488, catalogue number 115521), CD11c antibody (APC, catalogue number 117309), CD326 antibody (EpCAM, AF647, catalogue number 118212; APC, catalogue number 118214), CD80 (FITC, catalogue number 104706), CD86 (PE, catalogue number 105008) and Live/Dead staining Draq7 (catalogue number 424001) were purchased from BioLegend. Mouse IL-6 ELISA kit (catalogue number 88-7064-22) and mouse TNF-α ELISA kit (catalogue number 88-7324-22) were purchased from Thermo Fisher Scientific. Mouse IL-1β ELISA kit (catalogue number MLB00C-1) was purchased from R&D Systems.

LNP formulation

SiLNPs were prepared as follows. An ethanol phase containing all lipids and an aqueous phase containing mRNA (FLuc mRNA, Cre mRNA, FGF-2 mRNA or Cas9 mRNA/sgRNA) were mixed using a microfluidic device to formulate LNPs. The ethanol phase contained siloxane-incorporated lipidoids, DOPE, cholesterol and C14PEG2K with a fixed molar ratio of 35%, 16%, 46.5% and 2.5%, respectively. The aqueous phase was composed of RNA dissolved in 10 mM citrate buffer. The ethanol and aqueous phases were mixed at a flow rate of 1.8 ml min^{-1} and 0.6 ml min^{-1} (3:1) using Pump33DS syringe pumps. LNPs were dialysed in 1× PBS using a microdialysis cassette with a molecular weight cut-off (MWCO) of 20,000 Daltons (Thermo Fisher Scientific) for 2 h and then filtered through a 0.22 μm filter.

7C1 LNP was formulated utilizing 7C1 lipid, DOPE, cholesterol and C14PEG2K for the ethanol phase with a fixed molar ratio of 30%, 5%, 5% and 60%, respectively. 306Oi10 LNP was formulated utilizing 306Oi10 lipid, DOPE, cholesterol and C14PEG2K for the ethanol phase with a fixed molar ratio of 35%, 16%, 46.5% and 2.5%, respectively. 5A2-SC8-DOTAP LNP was formulated with 5A2-SC8 lipid, DOTAP, DOPE, cholesterol and DMG-PEG2000 for the ethanol phase with a fixed molar ratio of 11.9%, 50%, 11.9%, 23.81% and 2.38%, respectively. DLin-MC3-DMA (MC3) LNP was formulated with MC3 lipid, DSPC, cholesterol and C14PEG2K with a fixed molar ratio of 50%, 10%, 38.5% and 1.5%, respectively.

LNPs for large batch in vivo gene editing studies were formulated using a NanoAssemblr Ignite device. The ethanol phase and an aqueous phase were prepared as mentioned above, which was then mixed at a total flow rate of 12 ml min^{-1} (aqueous/ethanol flow rate ratio of 3/1) using a NanoAssemblr Ignite system. The mixture was then dialysed in 1× PBS using a microdialysis cassette with a molecular weight cut-off (MWCO) of 20,000 Daltons for 2 h. Resultant LNPs were concentrated with an Amicon Ultra 50K MWCO and filtrated through a 0.22 μm filter.

Characterization

^{1}H NMR spectra were obtained on a NEO 400 MHz spectrometer and analysed using MestReNova 9.0 software. LC-MS was performed using a Waters Acquity LCMS system equipped with UV–Vis and MS detectors. Flash chromatography was performed using a Teledyne Isco CombiFlash Rf-200i chromatography system equipped with UV–Vis and evaporative light scattering detectors. FT-IR spectra were obtained on a NICOLET iS50 FT-IR spectrometer. LNPs were formulated using a microfluidic device designed with herringbone features and a Pump33DS syringe pump (Harvard Apparatus) and/or a NanoAssemblr Ignite (Precision NanoSystems). Particle size and zeta potential were measured with a Malvern Zetasizer Nano ZS. Particle morphology was evaluated by cryo-TEM. A Zeiss LSM 710 confocal microscope with Zen 2011 blue edition software was used to evaluate GFP knock out in cells. A Leica SP8 microscope was used for immunofluorescence imaging of liver and lung tissues. Flow cytometry was performed using an LSR II, LSRFortessa or Symphony A3 Lite instrument (BD Biosciences). In vitro luminescence intensity, ALT qualification, AST qualification, TNS assay, BUN, triglyceride, creatinine tests and serum mTTR protein were quantified using an Infinite M Plex plate reader (Tecan).

Cell culture and animal studies

Dulbecco's modified Eagle medium (DMEM) was purchased from Gibco containing high glucose, L-glutamine and phenol red and without sodium pyruvate and HEPES. Trypsin-EDTA (0.25%) and penicillin/streptomycin (P/S) were purchased from Gibco. Fetal bovine serum (FBS) was purchased from Sigma-Aldrich. HepG2 (catalogue number HB-8065, ATCC), A549 (catalogue number CCL-185, ATCC), LLC (catalogue number CRL-1642, ATCC) and NIH/3T3 (catalogue number CRL-1658, ATCC) cells were cultured in DMEM supplemented with 10% FBS and 1% P/S. GFP-HepG2 cells were provided by John M. Maris Laboratory (University of Pennsylvania) and cultured in DMEM supplemented with 10% FBS and 1% P/S. DC2.4 cells were provided by Wei Guo Laboratory (University of Pennsylvania), who obtained it from Millipore (catalogue number SCC142), and cultured in RPMI1640 medium supplemented with 10% FBS and 1% P/S.

All animal protocols were approved by the Institutional Animal Care and Use Committee of University of Pennsylvania (protocol number 806540 and 806262) and were consistent with local, state and federal regulations as applicable. C57BL/6J (female and male, 6–8 weeks old), C57BL/6-Tg(CAG-EGFP)1Osb/J (female, 6–8 weeks old) and B6.Cg-Gt(ROSA)26Sortm14(CAG-tdTomato)Hze/J (Ai14, female, 6–8 weeks old) mice were purchased from Jackson Laboratory. All mice were used housed in a specific-pathogen-free animal facility at ambient temperature (22 ± 2 °C), air humidity 40–70% and 12 h dark/12 h light cycle and had free access to water and food. Animal health status was routinely checked by qualified veterinarians.

In vitro FLuc mRNA-LNP library screening

In a white wall transparent bottom 96-well plate, HepG2 cells were seeded at a density of 5×10^3 cells per well in 100 μl growth media (DMEM, 10% FBS, 1% P/S) and were incubated at 37 °C in 5% CO_2. The media were exchanged for fresh growth media, and then LNPs were treated at a dose of 10 ng FLuc mRNA per well. Luciferase expression was measured 24 h after LNP transfection using a luciferase assay system (Promega) according to the manufacturer's protocol. The luminescent signal was normalized to media-treated cells.

Membrane fluidity experiments

The membrane fluidity of Si_5-N14 and 213-N14 lipidoids was measured based on the fluorescence anisotropy of 7-methylcoumarin

(λ_{ex} = 315 nm, λ_{em} = 386 nm) from fluorescence polarization (Tecan F200 plate reader)[35]. 7-Methylcoumarin (10 µl, 100 µM) in DMSO was added into LNP (0.2 ml). The following equation was used to calculate the polarity (P):

$$P = (I_{0°0°} - GI_{0°90°})/(I_{0°0°} + GI_{0°90°})$$

$$G = I_{90°0°}/I_{90°90°}$$

Membrane fluidity was expressed as $1/P$ since polarity is inversely proportional to fluidity.

In vitro GFP knockout study

In a transparent 6-well plate, GFP-HepG2 cells were seeded at a density of 2×10^4 cells per well in 2 ml growth media (DMEM, 10% FBS, 1% P/S) and were incubated at 37 °C in 5% CO_2. The media were exchanged for fresh growth media, and then LNPs were treated at doses of 400, 800, 1,200, 1,600, 2,000, 4,000 and 6,000 ng Cas9 mRNA/GFP sgRNA (4/1, 3/1, 2/1, 1/1) per well. Media-treated cells and cells treated with Lipofectamine CRISPR MAX at the same Cas9 mRNA/GFP sgRNA dose were used as negative and positive controls, respectively. GFP knockout was measured 7 days after LNP treatment via flow cytometry on an LSR II instrument. The editing rate was calculated by normalizing GFP fluorescence intensity to media-treated groups.

In vivo FLuc mRNA-LNP delivery

Mice were treated with a single intravenous (i.v.) injection of FLuc mRNA LNPs. Luciferase expression was evaluated using an IVIS Spectrum imaging system (Caliper Life Sciences) 6 h post-injection (3 female mice for each group). Mice were then injected with D-luciferin (PerkinElmer) at a dose of 150 mg kg^{-1} via intraperitoneal (i.p.) injection. After 10 min of incubation under anaesthesia, bioluminescence intensity was quantified by measuring the photon flux in the region of interest using Living IMAGE 4 software provided by Caliper. Ex vivo imaging was performed on the heart, liver, spleen, lungs and kidneys after resection.

The pharmacokinetic profile of Si_5-N14 LNPs was studied as follows[26]: after administration of the Si_5-N14 LNP encapsulating FLuc mRNA to mice at an mRNA dose of 0.5 mg kg^{-1}, mice were euthanized at different time points and organs (liver, lungs and spleen) were collected. Tissue samples (~50 µg) were used for lipid extraction. After filtration, the extracted lipid samples were assessed using mass spectrometry. A standard curve was used to correlate the area under the curve of the extracted ion chromatograms to a quantitative amount of lipid.

In vivo Cre mRNA-LNP delivery

B6.Cg-Gt(ROSA)26Sortm14(CAG-tdTomato)Hze/J (Ai14) mice were treated with a single i.v. dose of Cre mRNA-LNPs at a dose of 0.3 mg kg^{-1} via tail vein injection (3 female mice for each group). To evaluate the per cent of tdTomato$^+$ cells in different cell types, cell isolation and staining was conducted 3 days post-injection, followed by flow cytometry analysis.

Mice were anaesthetized using isoflurane and then perfused with DMEM media containing collagen IV (0.5 mg ml^{-1}) and 1× PBS containing 0.1% BSA and 0.2% EDTA. Next, organs (liver, lungs and spleen) were collected and dissociated to collect liver cells. The obtained cell suspension was then centrifuged (5 min, 500 × g) and red blood cells were lysed using ACK lysis buffer (ThermoFisher) (1 ml) for 10 min. Afterwards, single-cell suspensions were obtained by centrifugation (5 min, 500 × g) and resuspended in 1× PBS (200 µl). To identify cell populations of interest, the antibodies used were anti-mouse Alexa Fluor (AF) 488 CD31 antibody (1:200, BioLegend, catalogue number 102514), Brilliant Violet (BV) 421 CD45 antibody (1:200, BioLegend, catalogue number 103134), AF 647 F4/80 antibody (1:200, BioLegend, catalogue number 123122), AF 647 CD326 antibody (1:200, EpCAM, BioLegend, catalogue number 118212), anti-mouse BV 421 F4/80 antibody (1:200, BioLegend, catalogue number 123137), AF 700 CD3 antibody (1:200, BioLegend, catalogue number 100216), AF 488 CD19 antibody (1:200, BioLegend, catalogue number 115521) and APC CD11c antibody (1:200, BioLegend, catalogue number 117309). The obtained single-cell suspensions were stained at 4 °C for 30 min with 2 µL of the above antibodies and afterwards were centrifuged, washed, centrifuged and resuspended in Draq7 dyed 1× PBS (1 ml, 0.1%) for flow cytometric analysis. Cell suspensions were analysed using a flow cytometer instrument (Symphony A3 Lite, LSRFortessa and LSR II) and subsequent data analysis was performed using FlowJo V10.

In vivo CRISPR–Cas9 m*TTR* editing in C57BL/6 mice

To perform liver m*TTR* gene knockout in vivo, C57BL/6J mice were treated i.v. with Si_4-C14b LNPs co-formulated with Cas9 mRNA and m*TTR* sgRNA at a total dose of 1.0 mg kg^{-1}, 2.0 mg kg^{-1} and 3.0 mg kg^{-1} (4/1, mRNA/sgRNA, wt/wt). MC3 and 306Oi10 LNPs encapsulating the same cargo were i.v. injected as positive controls and PBS was administered as a negative control (3 female mice for control groups, 4 female mice for the 306Oi10 LNP editing group, 5 female mice for the MC3 and Si_4-C14b LNP editing group). Blood was collected 1 day before injection and 7 days after injection, and serum was collected for TTR protein detection using an ELISA assay kit. The per cent of on-target *TTR* indels was analysed by next-generation sequencing. Liver tissue from the PBS group and liver-targeted Si_4-C14b-treated groups was analysed using ISH by the Histology Core at the Gene Therapy Program at the University of Pennsylvania.

In vivo CRISPR–Cas9 EGFP editing in the C57BL/6-Tg(CAG-EGFP)1Osb/J transgene mouse model

Si_5-N14 LNPs encapsulating Cas9 mRNA/EGFP sgRNA (4/1, wt/wt) were i.v. injected to C57BL/6-Tg(CAG-EGFP)1Osb/J (GFP, 3 female mice for each group) mice at a total RNA dose of 2.0 mg kg^{-1} (4 injections, dose 0.5 mg kg^{-1} per injection). Seven days post-injection, pieces of the lungs were collected and dissociated to collect lung cells. GFP knockout in the lung single-cell suspension was quantified using an LSRFortessa flow cytometer. Fluorescence-activated cell sorting (FACS) was performed on a BD FACSAria Fusion Sorter (BD Biosciences, FACS Diva v6). Lung tissue sections were prepared for immunostaining and subsequently imaged using a Leica DMi8 fluorescence microscope. Editing efficiency of sorted lung ECs was further evaluated using qPCR.

Immunofluorescence

For tissue sections, mouse liver and lungs was resected and transported to the laboratory on ice. Freshly dissected tissues were fixed, embedded and cut into 7 µm thick cryosections, and then postfixed with 3.2% PFA. Afterwards, tissue sections were blocked in PBS + 1% BSA, 5% donkey serum, 0.1% Triton X-100 and 0.02% sodium azide for 1 h at room temperature. Then, slides were incubated with primary antibodies (CD31 1:200, BioLegend, catalogue number 102502; ERG 1:2,000, Abcam, catalogue number ab92513; F4/80, Cell Signaling Technology, catalogue number 30325S; GFP antibody, ROCKLAND, catalogue number 600101215; VECad, R&D Systems, catalogue number AF1002) overnight at 4 °C. After that, slides were washed and incubated with fluorophore-conjugated secondary antibodies (Alexa Fluor 647-conjugated donkey anti-goat, 1:1,000, Thermo Fisher Scientific, catalogue number A-21447; Alexa Fluor 488-conjugated donkey anti-goat, 1:1,000, Thermo Fisher Scientific, catalogue number A-11055; Alexa Fluor 488-conjugated donkey anti-rabbit, 1:1,000, Thermo Fisher Scientific, catalogue number A-21206; Alexa Fluor 488-conjugated donkey anti-rat, 1:1,000, Thermo Fisher Scientific, catalogue number A-21208; Alexa Fluor 568-conjugated donkey anti-rat, 1:1,000, Thermo Fisher Scientific, catalogue number A78946; Alexa Fluor 647-conjugated donkey anti-rabbit, 1:1,000, Thermo Fisher Scientific, catalogue number A-31573) for 2 h. Lastly, slides were washed and incubated with 1 µM 4′,6-diamidino-2-phenylindole (DAPI) for 5 min

and mounted using ProLong Gold (Life Sciences, catalogue number P36930). Standard multiplex immunofluorescence images were taken with a Leica DMi8 microscope and analysed with LASX Office 1.4.6 software (Leica).

TTR on-target next-generation sequencing

DNA was extracted using a Qiagen Puregene Tissue Kit (catalogue number 158063) and quantified using a NanoDrop 2000. PCR amplification of the TTR target site was carried out using Q5 High-Fidelity DNA Polymerase (New England Biolabs M0491) using the following primer sequences: mTTR-exon2-F, 5′-CGGTTTACTCTGACCCATTTC-3′, and mTTR-exon2-R, 5′-GGGCTTTCTACAAGCTTACC-3′. Next-generation sequencing of the *TTR* amplicons was performed by the Nucleic Acids Technology Core, and determination of the on-target indel frequency was performed with modifications.

In vivo FGF-2 mRNA delivery in an influenza-induced lung vascular damage model

The lung vascular damage model was established as previously described[45]: influenza virus A/H1N1/PR/8 was administered intranasally at 50–60 TCID50 units to C57BL/6J mice (3 female mice for control groups, 4 female mice for FGF-2 mRNA-LNP-treated groups). Body weight and capillary blood oxygen were measured regularly at the desired time point. Capillary blood oxygen was measured by MouseOx Plus Small Animal Vital Signs Monitor and recorded by MouseOx Plus 2.0 Software (STARR Life Sciences Corp.). At day 15, the body weight of mice started to increase, and LNPs formulated with FGF-2 mRNA (0.5 mg kg^{-1}) were administered via tail vein injection. LNPs delivering FLuc mRNA with the same RNA dose and PBS were used as controls. Dexamethasone-21-phosphate (DEX) was injected intraperitoneally (i.p., 2 mg kg^{-1}) to the mice 30 min before LNP injection for all treatment groups. At day 25, mice were euthanized at the indicated time points for tissue collection.

In vivo CRISPR–Cas9 VEGFR2 editing in the LLC model

The LLC model was established via tail veil injection of 5×10^5 LLC cells to C57BL/6J mice (3 female and 2 male mice in each group); 14 days following tumour cell inoculation, mice were randomly assigned to three groups: PBS-treated controls (G1), Si_5-N14 LNPs encapsulating Cas9 mRNA/scramble sgRNA treatment (G2) and Si_5-N14 LNPs encapsulating Cas9 mRNA/VEGFR2 sgRNA treatment (G3). The sequence of VEGFR2 used was previously described[50]. Mice were treated every 3 days for a total of 3 injections (1 mg kg^{-1} of RNA per injection). Mice were euthanized 7 days post-administration of LNPs, and lungs were collected for analyses. It was noted that mice would be euthanized upon reaching a body weight loss exceeding 20% via carbon dioxide asphyxiation.

Endocytosis pathway of LNPs

To examine the cellular uptake mechanism, inhibition of endocytosis pathways was performed in iMVECs[51]. Cells treated with Si_5-N14 and 213-N14 LNPs encapsulating Cy5-tagged mRNA in the absence of inhibitors were used as controls. iMVECs were seeded into a 48-well plates at a density of 5×10^4 cells per well and incubated at 37 °C overnight. Then, the cells were washed with PBS, followed by pre-incubation at 37 °C for 1 h with one of the following endocytosis inhibitors dissolved in DMEM media: amiloride (AMI), chlorpromazine (CMZ), genistein (GEN) and methyl-β-cyclodextrin (βCD). Then, the media were removed and replaced with DMEM media containing LNPs (mRNA dose 100 ng ml^{-1}) for another 30 min. Cells were then washed and collected for flow cytometric analysis.

Isolation of protein corona absorbed to LNPs

Isolation of the protein corona absorbed to LNPs was conducted as previously described[25,26]. Briefly, mouse whole blood was collected into EDTA-treated tubes and then centrifuged at 1,000 × *g* at 4 °C for 10 min to obtain mouse plasma. To ensure the lack of protein aggregates in the sample, mouse plasma was centrifuged at 13,000 × *g* at 4 °C before use. LNPs were mixed with mouse plasma at a 1:1 volume ratio and incubated for 1 h at 37 °C under gentle shaking. The supernatant was removed, and the pellet was washed with cold 1× PBS. Next, the pellet was centrifuged again for 5 min at 13,000 × *g* at 4 °C, and the supernatant was removed. This washing step was performed three times before resuspending the final pellet in 1× PBS. The same procedure was performed for plasma aliquots without LNPs to verify the absence of protein precipitation. The amount of protein in protein corona-coated LNPs was determined using a BCA assay kit before protein corona analysis by The Wistar Institute's Proteomics and Metabolomics Core.

Simulation of lipidoids and lipid head

The ALog *P* values of the Si_5-N14 and 213-N14 lipidoids were predicted from atomic physiochemical properties. Head radius calculation of the Si_5-N14 and 213-N14 lipidoids was optimized at the CHARMM force field[52]. Lipid simulations were run for up to 4,000 steps to achieve energy-minimized structures. All bonds containing intermolecular interactions were constrained using the Smart Minimizer algorithm. The overall Root-Mean-Squared gradient tolerance was set to 0.01.

Statistics and reproducibility

Two-sided Student's *t*-test or one-way analysis of variance (ANOVA) followed by Dunnett's multiple comparison test was applied for comparison between two groups or among multiple groups using GraphPad Prism 9.0, respectively. $P < 0.05$ was considered to be statistically significant. Each experiment is repeated at least three times independently with similar results, and the representative dataset is presented.

Reporting summary

Further information on research design is available in the Nature Portfolio Reporting Summary linked to this article.

Data availability

All relevant data supporting the findings of this study are available within the paper, Supplementary Information or Source Data file. Source data are provided with this paper.

References

50. Huang, X. et al. Genome editing abrogates angiogenesis in vivo. *Nat. Commun.* **8**, 112 (2017).
51. Wei, T. et al. Systemic nanoparticle delivery of CRISPR-Cas9 ribonucleoproteins for effective tissue specific genome editing. *Nat. Commun.* **11**, 3232 (2020).
52. Momany, F. & Rone, R. Validation of the general purpose QUANTA ®3.2/CHARMm® force field. *J. Comput. Chem.* **13**, 888 (1992).

Acknowledgements

M.J.M. acknowledges support from a US National Institutes of Health (NIH) Director's New Innovator Award (DP2 TR002776), a Burroughs Wellcome Fund Career Award at the Scientific Interface (CASI), an American Cancer Society Research Scholar Grant (RSG-22-122-01-ET), a US National Science Foundation CAREER Award (CBET-2145491) and the National Institutes of Health (NICHD R01 HD115877). A.E.V. acknowledges support from NIH grants (R01HL153539) and the Margaret Q. Landenberger Foundation. S.J.S. and K.L.S. are supported by an NSF Graduate Research Fellowship (award 1845298). R.P. was supported by an NIH F30 fellowship (F30HL162465-01A1). Z.X. is supported by a CRI Irvington fellowship (grant number CRI4168) from the Cancer Research Institute. We thank The Wistar Institute, the Pathology Core, Nucleic Acids Technology Core, and Program for Comparative Medicine at the Gene Therapy Program for technical assistance and I. Muthuramu for analysis of deep sequencing data. Elements in Figs. 1, 4, 5 and 6 were created with BioRender.com.

Author contributions

L.X. and M.J.M. conceived the concept. L.X. and X.X. designed and synthesized all the siloxane-incorporated ionizable lipids used in this study. L.X., N.G., G.Z., X.H., C.C.W., V.C., R.P., R.E.-M. and Y.S. performed the experiments. L.X., N.G., S.J.S., K.L.S., K.W. and M.J.M. wrote the paper. L.X., G.Z., N.G., X.H., S.J.S., X.X., Z.X., R.P., J.X., K.L.S., C.C.W., R.E.-M., V.C., I.-C.Y., J.X., J.C., Y.S., M.-G.A., K.W., L.W., D.J.P., D.W., A.E.V., J.M.W. and M.J.M. reviewed and commented on the paper.

Competing interests

L.X. and M.J.M. are inventors on a patent filed by the Trustees of the University of Pennsylvania (International Patent Application No. PCT/US23/66564) describing the lipid nanoparticle technology in this study. J.M.W. is a paid advisor to and holds equity in iECURE, Passage Bio and the Center for Breakthrough Medicines (CBM). He also holds equity in the former G2 Bio asset companies and Ceva Santé Animale. He has sponsored research agreements with Alexion Pharmaceuticals, Amicus Therapeutics, CBM, Ceva Santé Animale, Elaaj Bio, FA212, Foundation for Angelman Syndrome Therapeutics, former G2 Bio asset companies, iECURE and Passage Bio, which are licensees of Penn Technology. J.M.W., L.W. and C.C.W are inventors on patents that have been licensed to various biopharmaceutical companies and for which they may receive payments. D.W. is named on patents that describe the use of nucleoside-modified mRNA as a platform to deliver therapeutic proteins and vaccines. M.J.M., D.W. and M.-G.A. are also named on patents describing the use of lipid nanoparticles and lipid compositions for nucleic acid delivery. The other authors declare no competing interests.

Additional information

Extended data is available for this paper at https://doi.org/10.1038/s41565-024-01747-6.

Supplementary information The online version contains supplementary material available at https://doi.org/10.1038/s41565-024-01747-6.

Correspondence and requests for materials should be addressed to Michael J. Mitchell.

Peer review information *Nature Nanotechnology* thanks Yusuke Sato and the other, anonymous, reviewer(s) for their contribution to the peer review of this work.

https://doi.org/10.1038/s41565-024-01747-6

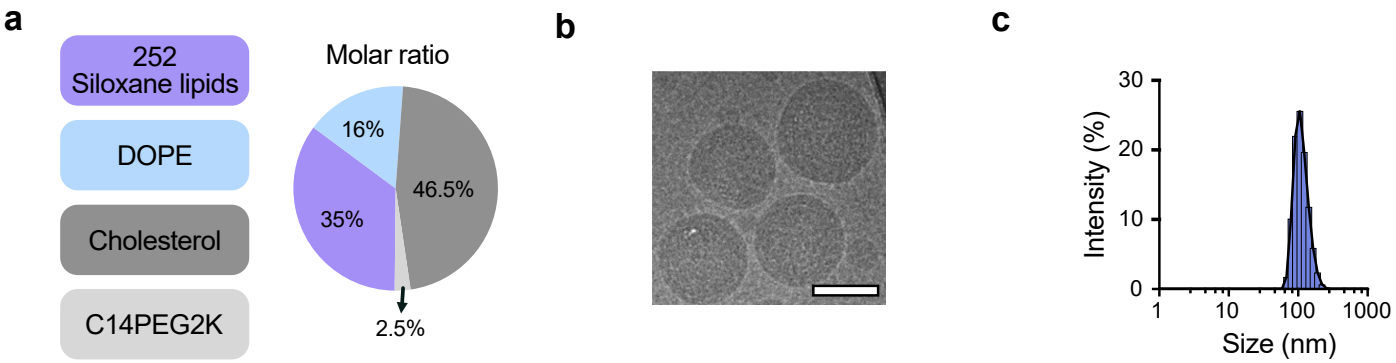

Extended Data Fig. 1 | Formulation parameters and characterization of SiLNPs. a, SiLNPs formulation parameters. Siloxane-incorporated lipidoids, DOPE, cholesterol, and C14PEG2K with molar ratio of 35%, 16%, 46.5%, and 2.5% were used for SiLNPs formulation. **b**, Representative cryogenic transmission electron microscopy (cryo-TEM) image of SiLNP morphology. Scale bar: 100 nm. **c**, Hydrodynamic size distribution of representative SiLNP.

https://doi.org/10.1038/s41565-024-01747-6

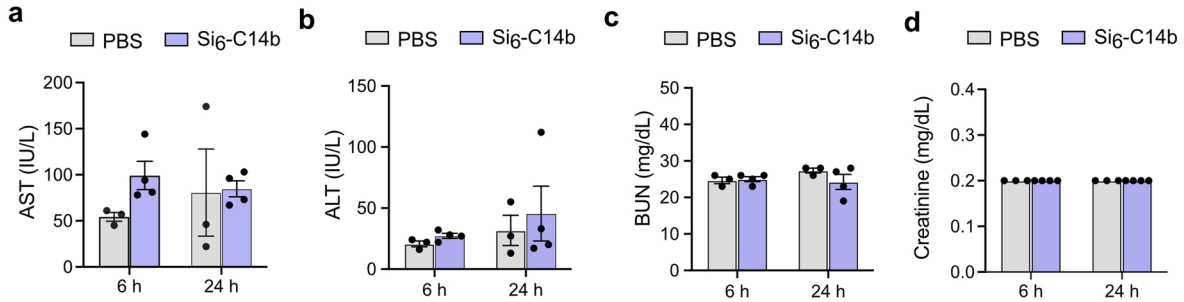

Extended Data Fig. 2 | Blood chemistry evaluation of mice after administration of Si_6-C14b LNP co-delivering Cas9 mRNA and TTR sgRNA. (**a**) AST, (**b**) ALT, (**c**) BUN, and (**d**) Creatinine levels of blood samples obtained from mice treated with PBS and Si6-C14b LNP (RNA dose: 3 mg kg^{-1}). Data are presented as mean ± s.e.m. (n = 3 mice for PBS treated groups; n =4 for LNP treated groups).

nature portfolio

Corresponding author(s): Michael Mitchell

Last updated by author(s): Jun 11, 2024

Reporting Summary

Nature Portfolio wishes to improve the reproducibility of the work that we publish. This form provides structure for consistency and transparency in reporting. For further information on Nature Portfolio policies, see our Editorial Policies and the Editorial Policy Checklist.

Statistics

For all statistical analyses, confirm that the following items are present in the figure legend, table legend, main text, or Methods section.

n/a	Confirmed	
☐	☒	The exact sample size (*n*) for each experimental group/condition, given as a discrete number and unit of measurement
☐	☒	A statement on whether measurements were taken from distinct samples or whether the same sample was measured repeatedly
☐	☒	The statistical test(s) used AND whether they are one- or two-sided *Only common tests should be described solely by name; describe more complex techniques in the Methods section.*
☐	☒	A description of all covariates tested
☐	☒	A description of any assumptions or corrections, such as tests of normality and adjustment for multiple comparisons
☐	☒	A full description of the statistical parameters including central tendency (e.g. means) or other basic estimates (e.g. regression coefficient) AND variation (e.g. standard deviation) or associated estimates of uncertainty (e.g. confidence intervals)
☐	☒	For null hypothesis testing, the test statistic (e.g. *F*, *t*, *r*) with confidence intervals, effect sizes, degrees of freedom and *P* value noted *Give P values as exact values whenever suitable.*
☒	☐	For Bayesian analysis, information on the choice of priors and Markov chain Monte Carlo settings
☒	☐	For hierarchical and complex designs, identification of the appropriate level for tests and full reporting of outcomes
☒	☐	Estimates of effect sizes (e.g. Cohen's *d*, Pearson's *r*), indicating how they were calculated

Our web collection on statistics for biologists contains articles on many of the points above.

Software and code

Policy information about availability of computer code

Data collection	ZEN2011, MestReNova 9.0, Flowjo V10, IVIS specturm, LAS X software (Leica), ImageJ software, MouseOx® Plus Software (STARR Life Sciences Corp.)
Data analysis	Small animal imaging data were analyzed by the Living Image 4 Software (Caliper Life Sciences). Confocal fluorescence microscopy imaging data were collected using Zen 2011 blue edition (Carl Zeiss). Endosomal escape was analyzed with ImageJ 1.54f software. Fluorescent microscopy imaging data were analyzed using LASX Office 1.4.6 (Leica). All statistical calculations were performed using GraphPad Prism 9.0 (GraphPad Software Inc.) NMR spectra were analyzed using Mestre Nova 9.0 (Mestre lab Research S.L.). Flow cytometry results were analyzed by FACS Diva v6 and FlowJo V10. Capillary blood oxygen was measured by MouseOx® Plus Small Animal Vital Signs Monitor and recorded by MouseOx® Plus 2.0 Software (STARR Life Sciences Corp.).

For manuscripts utilizing custom algorithms or software that are central to the research but not yet described in published literature, software must be made available to editors and reviewers. We strongly encourage code deposition in a community repository (e.g. GitHub). See the Nature Portfolio guidelines for submitting code & software for further information.

Data

Policy information about availability of data

All manuscripts must include a data availability statement. This statement should provide the following information, where applicable:

- Accession codes, unique identifiers, or web links for publicly available datasets
- A description of any restrictions on data availability
- For clinical datasets or third party data, please ensure that the statement adheres to our policy

The authors declare that all relevant data supporting the finding of this study are available within the article, Supplementary Information or Source Data file. Source data are provided with this paper.

Human research participants

Policy information about studies involving human research participants and Sex and Gender in Research.

Reporting on sex and gender	N/A
Population characteristics	N/A
Recruitment	N/A
Ethics oversight	N/A

Note that full information on the approval of the study protocol must also be provided in the manuscript.

Field-specific reporting

Please select the one below that is the best fit for your research. If you are not sure, read the appropriate sections before making your selection.

☒ Life sciences ☐ Behavioural & social sciences ☐ Ecological, evolutionary & environmental sciences

For a reference copy of the document with all sections, see nature.com/documents/nr-reporting-summary-flat.pdf

Life sciences study design

All studies must disclose on these points even when the disclosure is negative.

Sample size	No effect size was predetermined, but sample sizes employed in this study are consistent with previously published works (Li A W, Sobral M C, Badrinath S, et al. Nature materials, 2018, 17(6): 528-534; or Kuai R, Ochyl L J, Bahjat K S, et al. Nature materials, 2017, 16(4): 489-496.). For example, in vitro studies were repeated at least three times independently and in the in vivo experiments with at least 3 mice per group were performed.
Data exclusions	No data was excluded from the analysis.
Replication	Experiments were repeated at least three independent experiments with similar results. All experiments were reproduced to reliably support conclusions stated in the manuscript.
Randomization	For the in vivo FLuc and Cre mRNA delivery, cages of mice were randomly selected and then divided into experimental groups for further in vivo dosing treatment. For CRISPR-Cas9 gene editing studies, cages of mice were randomly selected and then divided into experimental groups for dosing treatment. For lung tumor model, mice with similar weight were randomly subjected for tumor cell inoculation. On day 14, mice were randomly assigned to three groups for treatment. For lung vascular damage model, mice with similar weight were randomly administered with influenza virus. On day 15, mice were randomly assigned into three groups for therapeutic treatment.
Blinding	Investigators were blinded to group allocation during experiments. Investigators performing in vivo luminescence and gene editing were blinded to saline and mRNA-LNPs treatment groups during data collection and analysis.

Reporting for specific materials, systems and methods

We require information from authors about some types of materials, experimental systems and methods used in many studies. Here, indicate whether each material, system or method listed is relevant to your study. If you are not sure if a list item applies to your research, read the appropriate section before selecting a response.

Materials & experimental systems

n/a	Involved in the study
☐	☒ Antibodies
☐	☒ Eukaryotic cell lines
☒	☐ Palaeontology and archaeology
☐	☒ Animals and other organisms
☒	☐ Clinical data
☒	☐ Dual use research of concern

Methods

n/a	Involved in the study
☒	☐ ChIP-seq
☐	☒ Flow cytometry
☒	☐ MRI-based neuroimaging

Antibodies

Antibodies used

BV421 anti-mouse CD45 (1:200, Cat#103134), AF488 anti-mouse CD31 (1:200, Cat#102514), AF647 anti-mouse F4/80 (1:200, Cat#123122), AF647 anti-mouse CD326 (EPCAM, 1:200, Cat#118212), BV421 anti-mouse F4/80 (1:200, Cat#123137), AF700 anti-mouse CD3 (1:200, Cat#100216), AF488 anti-mouse CD19 (1:200, Cat#115521), APC anti-mouse CD11c (1:200, Cat#117309), PE anti-mouse CD31 (1:200, Cat#102508), APC anti-mouse CD326 (EPCAM, 1:200, Cat#118214), FITC anti-mouse CD80 antibody (1:200, Cat#104705) and PE anti-mouse CD86 antibody (1:200, Cat#105007) were purchased from Biolegend. Primary antibodies were: CD31, 1:200, BioLegend, Cat#102502; ERG 1:2000, Abcam, Cat#ab92513; F4/80, Cell Signaling Technology, Cat#30325S; GFP antibody, 1:1000, ROCKLAND, Cat#600101215; VECad, 1:200, R&D system, Cat#AF1002. Secondary antibodies were: Alexa Fluor™ 647-conjugated donkey anti-goat, 1:1000, Thermo Fisher Scientific, Cat#A-21447; Alexa Fluor™ 488-conjugated donkey anti-goat, 1:1000, Thermo Fisher Scientific, Cat#A-11055; Alexa Fluor™ 488-conjugated donkey anti-rabbit, 1:1000, Thermo Fisher Scientific, Cat#A-21206; Alexa Fluor™ 488-conjugated donkey anti-rat, 1:1000, Thermo Fisher Scientific, Cat#A-21208; Alexa Fluor™ 568-conjugated donkey anti-rat, 1:1000, Thermo Fisher Scientific, Cat#A78946; Alexa Fluor™ 647-conjugated donkey anti-rabbit, 1:1000, Thermo Fisher Scientific, Cat#A-31573.

Validation

All antibodies used in the study were commercial and validated by the manufacturer. Species and application validations and citations for primary antibodies can be found from the manufacturer's websites.

Eukaryotic cell lines

Policy information about cell lines and Sex and Gender in Research

Cell line source(s)

HepG2, A549, and NIH/3T3 cells were purchased from the American Type Culture Collection (ATCC). GFP-HepG2 cell were provided by Dr. Maris (UPenn). iMVECs were provided by Dr. Vaughan (UPenn). DC2.4 cells were provided by Wei Guo Laboratory (UPenn), who obtained it from Millipore (Cat#SCC142). Lewis Lung Carcinoma (LLC) were provided by Ellen Puré Laboratory (UPenn), who obtained it from ATCC (Cat#CRL-1642). All of the cell lines were tested negative for mycoplasma in University of Pennsylvania cell center.

Authentication

A short tandem repeat DNA profiling method was used to authenticate the cell lines and the results were compared with reference database. There is no mycoplasma contamination in the above cell lines.

Mycoplasma contamination

All cell lines were tested for mycoplasma contamination. No mycoplasma contamination was found.

Commonly misidentified lines
(See ICLAC register)

These cell lines we used were not listed in commonly misidentified lines in ICLAC Register.

Animals and other research organisms

Policy information about studies involving animals; ARRIVE guidelines recommended for reporting animal research, and Sex and Gender in Research

Laboratory animals

C57BL/6 mice (female & male, 6-8 weeks), C57BL/6-Tg(CAG-EGFP)1Osb/J mice (female, 6-8 weeks), and B6.Cg-Gt(ROSA)26Sortm14 (CAG-tdTomato)Hze/J mice (female, 6-8 weeks) were ordered from Jackson laboratory and housed in a specific-pathogen-free animal facility at ambient temperature (22 ± 2 °C), air humidity 40%–70% and 12-h dark/12-h light cycle.

Wild animals

No wild animal was involved in this study.

Reporting on sex

Female and male mice were used in this study

Field-collected samples

The study did not involve samples collected from the field.

Ethics oversight

All animal experiment protocols were reviewed and approved by the institutional animal care and use committee of the University of Pennsylvania.

Note that full information on the approval of the study protocol must also be provided in the manuscript.

Flow Cytometry

Plots

Confirm that:

☒ The axis labels state the marker and fluorochrome used (e.g. CD4-FITC).

☒ The axis scales are clearly visible. Include numbers along axes only for bottom left plot of group (a 'group' is an analysis of identical markers).

☒ All plots are contour plots with outliers or pseudocolor plots.

☒ A numerical value for number of cells or percentage (with statistics) is provided.

Methodology

Sample preparation	Details of sample preparation are provided in the Supplementary Information, including tissue-processing steps. Briefly, tissues samples were chemically disruption and filtered through a 70 μM strainer. Then the suspensions were incubated with ammonium chloride buffer for erythocyte lysis and washed with PBS. Single-cell suspensions were obtained and stained with antibodies according to the manufacturer's protocols, and then analyzed by flow cytometry.
Instrument	BD LSR II, LSRFortessa, Symohony A3 Lite (BD Biosciences)
Software	FACS Diva v6 and FlowJo V10
Cell population abundance	The absolute cells around 100000 were analyzed for fluorescent intensity in the defined gate.
Gating strategy	Briefly, single cells were selected by FSC and SSC plots. Live cells were selected as defined by Live Dead Stain-negativity. Immune cells were gated by CD45+ cells. Macrophages were gated by F4/80+ cells. Endothelial cells were gated by CD45-/CD31+ cells. Epithelial cells were gated by CD45-/CD31-/ CD326+ cells. B cells were gated by CD19+ cells. T cells were gated by CD3+ cells. Dendritic cells were gated by CD11c+ cells. Detailed gating strategies were provided in the Supplementary Information Figures 29, 35, 39, and 47.

☒ Tick this box to confirm that a figure exemplifying the gating strategy is provided in the Supplementary Information.